

Global hydro-climatic biomes via mulit-task learning

Christina Papagiannopoulou, Diego G. Miralles, Matthias Demuzere, Niko E. C. Verhoest, Willem Waegeman

Authors' response to the Referees

For clarifying our answers to the reviewers' comments, the following scheme is used: comments of the reviewers are denoted in plain font, our answers are denoted in **bold** font and quotes from the manuscript are denoted in ***bold italic***. We also number the different comments of the reviewers as: I.J, where I is the number of the referee and J the number of the remark.

Response to the comments of Stephanie Horion

The work presented by Papagiannopoulou et al. in this manuscript is of interest for the reader of GMD and is also very relevant for the ecosystem and climate research community. Overall the manuscript is well structured and the methodology section generally well documented. Knowing that the focus of GMD is on the progress and novelty in computation and model development, I support the need for in-depth description of the MTL model and its performances (e.g. STL vs MTL, capability to detect Granger causality, etc.). However I believe that the manuscript would be strengthened and results better supported if the authors could really demonstrate that the new product (i.e. map of hydro-climatic biomes) is outperforming other bio-climatic maps that did not consider in their design the vegetation response to climate variability. This is still lacking in the current manuscript. In addition some methodological aspects that led to the final design of the MTL and clustering should also be improved to backup the authors statement on the performances of the final models and derived product. Based on these observations and on the detailed comments provided below I recommend the paper for major revision.

We would like to thank the reviewer for her appreciation of our manuscript, the constructive feedback, and thorough assessment. Below we provide a point-by-point response to each comment.

In general, we would like to clarify that the goal of our study is to provide a new methodology that can identify coherent regions in which vegetation responds to climate in a similar way. We model our problem with a multi-task learning approach that considers the different locations as different tasks and learns the relationship between the tasks during the learning process. Hence, the climate-vegetation interaction is simultaneously learned for all locations. The similarity between the learned relationships (between the tasks) is also discovered during the process. This is the first time (to the best of our knowledge) that an approach of this kind, which discovers the structure of the relationships between the different locations at global

scale, is applied on this setting. As such, we try to avoid the claim that our *hydro-climatic biomes* ‘outperform’ other schemes, which rely on climate and/or vegetation data and not on the modelled interaction between climate and vegetation. It is not really our intent to outperform these land cover classifications, and the comparison that is provided against them is to assure that – despite the fact that our approach does not prescribe any explicit information on land cover types – comparable regions arise from our data-guided appraisal.

Specific comments

Introduction

1.1) Studying vegetation response to climate variability is and has been the focus of numerous researches. I know the objective of the authors is to create a new bio-climatic map, however I can imagine that their work build up on recent developments in science regarding ecosystem response to climate variability. This is not well reflected in the introduction. Please add some references to key papers, studies in the matter. Some suggestions below:

Liu L, Zhang Y, Wu S, Li S, Qin D (2018) Water memory effects and their impacts on global vegetation productivity and resilience. *Sci Rep*, 8, 2962.

Seddon AW, Macias-Fauria M, Long PR, Benz D, Willis KJ (2016) Sensitivity of global terrestrial ecosystems to climate variability. *Nature*, 531, 229-232.

De Keersmaecker W, Lhermitte S, Tits L, Honnay O, Somers B, Coppin P (2015) A model quantifying global vegetation resistance and resilience to short-term climate anomalies and their relationship with vegetation cover. *Global Ecology and Biogeography*, 24, 539-548.

Nemani RR, Keeling CD, Hashimoto H et al. (2003) Climate-driven increases in global terrestrial net primary production from 1982 to 1999. *Science*, 300, 1560-1563

We have included the suggested literature in the revised manuscript.

p2.23: *Previous studies rely on spectral information, supervised techniques or clustering approaches, which are applied to observations of climate variables and/or vegetation characteristics. However, these classification schemes are not based on the type of response of vegetation to climate dynamics. Recent advances in understanding vegetation response to climate variability highlight the importance of revealing the sensitivity of ecosystems to climate conditions, see Nemani et al. (2003); De Keersmaecker et al. (2015); Seddon et al. (2016); Papagiannopoulou et al. (2017); Liu et al. (2018). Therefore, a step beyond these previous studies is a spatial characterization of the vegetation dynamics that are induced by climate variability, so that ecosystems of similar response to climate anomalies can be unveiled.*

1.2) The authors claim (p2, l23) that it is the first time that ecoregions are

being defined based on the analysis of vegetation response to climate variability. I agree that the idea is relatively novel and definitely relevant. Yet previous attempts have been made, notably by combining PCA and clustering techniques applied to climate and vegetation dataset. See the following reference as an example:

Ivits E, Horion S, Fensholt R, Cherlet M (2014) Global Ecosystem Response Types Derived from the Standardized Precipitation Evapotranspiration Index and FPAR3g Series. *Remote Sensing*, 6, 4266-4288.

Thanks for pointing us to this paper. The reference is relevant to our study and has been referred to in the revised version. The differences compared to this and other studies have been also highlighted in the revised version.

p2.34: *A previous effort towards detecting regions with similar vegetation response to climate involves the work of Ivits et al. (2014), where PCA is performed on the data matrix of drought anomalies and vegetation state, and a clustering is applied to the correlation coefficients based on the spatio-temporal patterns obtained by PCA. However, in this study, the interaction between climate and vegetation is not explicitly learned, nor the causes behind vegetation changes are inferred in a predictor-target framework.*

Methodology

1.3) Sect. 2.4. The authors mentioned that the ASO method used here should not be confused with PCA. It would be useful to develop this statement. Indeed for both techniques orthonormal vectors are derived from the high dimensional feature space, creating a new ‘optimized’ low-dimensional feature space. The authors mentioned that the goal of the ASO method is to detect the PC of the predictive structure. Knowing that PCA can be performed in two ways (t-mode and s-mode), the t-mode being the most frequently used by climatologist to identify recurrent spatial patterns over time, whereas the S-mode allows for identifying recurrent temporal patterns over space. How would the current method differ from an extended PCA in S-mode? I can imagine that using EPCA over a dataset as large as the one used here could be a real challenge for example. But I would like the authors to elaborate on the pros and cons of the new method as compared to already established techniques in the climate research such as PCA/EPCA for example.

In the last paragraph of Sect. 2.4, we mentioned the main difference between the commonly-used PCA approaches and the proposed method. However, we have elaborated on the differences and potential advantages of our approach in the revised manuscript by extending Sect. 2.4 and adding relevant literature.

p8.7: *The SVD-based ASO method can be interpreted as a dimensionality reduction technique applied to the model space (i.e., weights). It should be stressed here that this method must not be confused with principal component analysis (PCA), which is usually employed on the data space (input space of predictors) (Metzger et al., 2012; Ivits et al., 2014). The goal of the ASO method is to detect the principal components of the parameter matrix, while PCA identifies the principal components of the input data X. The goal of the ASO method can be achieved by considering the models of multiple tasks as samples of their own distribution. Therefore, these samples can only be formed by using an MTL approach, in which there is access to the models from multiple learning tasks. Moreover, in our work, we explicitly consider the climatic variables as predictors and the vegetation variable as target variable, and we learn the relationship between them in a supervised setting. As such, the regions that we define rely on the relationship between climate and vegetation in a prediction setting, and the clustering is calculated based on similarity of this relationship (i.e. the model coefficients for different locations), see Sect. 2.5 for more details. As such, we learn relationships between climate and vegetation in a supervised setting, whereas PCA-based methods (Metzger et al., 2012; Ivits et al., 2014) are fully unsupervised. In our study the SVD decomposition is used as part of the optimization algorithm, thus in a supervised setting. In this setting, the model weights are optimized based on a given training set. Therefore, the discovered structures are obtained during the training process.*

1.4) Sect. 2.5. The authors do not give any name or reference for the clustering technique used here. Please clarify if a new algorithm has been developed for the study or if an already developed clustering technique was applied.

In the manuscript, it is mentioned that the clustering technique that we use is the agglomerative hierarchical clustering (with Euclidean distance measure). This is a well-known clustering method in Statistics (see Sect. 2.5 and 3.2 of the manuscript). To make it more clear to the broad audience of GMD, we have mentioned in the revised manuscript that we used the hierarchical clustering python implementation of scikit-learn, and added a specific reference.

p10.32: *In our application, we use a hierarchical agglomerative clustering approach (Ward, 1963) where the number of clusters is not predefined.*

p17.26: *We use the implementation of Python for the L-BFGS optimizer, the singular value decomposition method and the hierarchical clustering (scikit-learn python library (Pedregosa et al., 2011)).*

1.5) General comment on the use of R^2 for assessing the model performance: at several occasions (in the manuscript and in the supplementary material), the authors used R^2 to quantify the performance of different models (MTL vs. STL, models with and without Granger causality, inclusion of higher-level features in the input dataset, final decision on the number of clusters). They generally conclude that the best model is the one with the highest R^2 . I agree on the principle, however looking at the differences between R^2 (e.g. figures 3b and 3d, large areas present difference in R^2 below 0.1), I wonder whether all these differences are statistically significant. As based on the analysis of R^2 , the authors are deciding on the final set of input data, the final design of the MTL model, and the final number of clusters, I would really urge the need for further statistical assessment of the model performances. One first analysis could simply be to estimate the percentage area of pixels with statistically significant increase in R^2 .

The distributions depicted in Figs. 3c and 3f of the manuscript show that the results of the MTL and STL methods are substantially different. Specifically, the distributions of the MTL results are shifted to the right, meaning that STL is outperformed by MTL at global scale. This result can be confirmed by any paired statistical test (Demšar, 2006). The results of the Wilcoxon non-parametric statistical test are included in the revised manuscript.

At pixel level, traditional statistical tests usually have too many assumptions for our purposes. Alternatively, non-parametric tests based on resampling, such as permutation or bootstrap tests, cannot really be applied due to the size of our data set. A proposed solution is to use the Diebold-Mariano statistical test (Diebold, 2015). This test has been used to compare the MTL and the STL approaches in the revised version of the manuscript.

For the final decision about the number of clusters, see our answer in comment 1.6.

p13.6: *The dotted regions in Fig. 3b correspond to areas where the MTL model significantly outperforms the STL models based on the Diebold-Mariano statistical test, which compares model predictions (Diebold, 2015). For the statistical test, we use the False Discovery Rate (Benjamini and Hochberg, 1995) method to correct the p-values at level 0.05 due to the multiple-hypothesis testing setting.*

p13.16: *As it can be observed, the distribution of the R^2 scores is shifted to the right for the MTL, meaning that values are typically greater than those derived from the STL approach. Moreover, the skew towards the left in the blue histogram, with values close to zero, is an indication of the near-zero performance of the STL models in many locations. The Wilcoxon paired statistical test (Demšar, 2006) confirms that the results of the two approaches are statistically dif-*

ferent ($p\text{-value} < 10^{-9}$).

p13.27: *In this figure it becomes clear that climate dynamics Granger-cause monthly vegetation anomalies in most regions of the world, and the ability of the MTL model to detect deterministic relationships is evidenced. This is also confirmed by the Wilcoxon paired statistical test ($p\text{-value} < 10^{-9}$).*

p13.33: *Analogous to Fig. 3c, Fig. 3f compares the distributions of Granger causality (i.e., the difference in predictive performance in terms of R^2 between the full and the baseline model) between the STL and MTL approach. Once again, the blue histogram corresponds to the distribution of Granger causality retrieved using the STL approach, while the orange corresponds to the results of the MTL approach. The shift to the right of the orange histogram shows the larger ability of the MTL model to reveal Granger-causality between climate and vegetation. Similar to the previous comparison, the Wilcoxon paired statistical test (Demšar, 2006) confirms that the results of the two approaches are statistically different ($p\text{-value} < 10^{-9}$). See Sect. 3.1 and Fig. 3b.*

Results

1.6) General comment on the final number of clusters: the fact that the majority of the Iberian Peninsula is included in the transitional energy driven cluster together with Ireland, an important part of SE Asia, part of Brasil and Venezuela Colombia makes me wonder if a higher number of clusters would not be more appropriate. The authors mentioned already in Figure S2 that the differences in the predictive performance for $h = 6 - 15$ are marginal. Further assessments should therefore be performed in order to identify the optimal number of hydro-climatic biomes. Part of this assessment should be dedicated to the understanding of the actual drivers (main predictors) for each biome. I believe providing a solid justification for the naming of the different biomes (by referring back to the main predictors) would be beneficial for the paper.

We agree that the differences in predictive performance for $h = 6-15$ are marginal. However, the proposed method is a fully data-driven approach that is not fine-tuned based on any kind of prior knowledge. Therefore, the selection of the final value of the h parameter is based on an objective criterion, i.e. the model performance. As for the resulting map (Fig. 4a), although we are aware that this map may not fully reflect all particular expectations, we do believe that the spatial distribution broadly captures the expected regimes of climate–vegetation interactions, as described in the results section. Note as well that in our early experiments we ran our approach with a different number of clusters to visually inspect the resulting regions. The

regions formed with h values close to 11 are similar to the reported ones (Fig. 4a of the manuscript). This result proves the robustness of the proposed method to detect the basic vegetation response types with respect to climate. The results (for $h = 9-12$) have been included as supplementary figures in the revised manuscript.

Concerning the label scheme, we should stress that the names of the biomes are inspired by the main predictors based on Papa-
giannopoulou et al. (2017). We are afraid that making the labels reflect these predictors more accurately would make them extremely complex and rather impractical. So we preferred to keep this label scheme in the revised manuscript.

p1.16 of Supplement: *Therefore, we can conclude that the method gives robust results as the strongest predictive structures are captured for the first most important components given by the singular value decomposition. This conclusion is also confirmed by Fig. S3, where the maps with 9 (Fig. S3a), 10 (Fig. S3b), 11 (Fig. S3c) and 12 (Fig. S3d) hydro-climatic biomes are depicted. In all figures, the tropics, the boreal and the arid regions are well-detected. In addition, sub-tropical regions and transitional ones are also commonly defined in all of the aforementioned figures. Differences in the borders of the identified regions are noticed between temperature-driven areas (e.g., Europe and North America). In transitional water- and energy-driven regions also there are some differences in the clusters borders. However, these inconsistencies can be explained by the smoother differences between the climatic and environmental conditions in these areas.*

See Fig. S3 of Supplementary material.

1.7) In relation to the previous comment, how does the new global map of hydro-climatic biomes perform as compared to previous ones (not including information of vegetation condition and response to climate)? It would be really interesting if the authors could showcase for one (or more) bio-climatic zone how the new bio-climatic zone provide a finer, more accurate picture of global terrestrial biomes by analysis the specific (/sub-local) ecosystem response to climate variability. To this regard, the bioclimatic map produced by Metzger et al. (see reference below) could also be of interest for comparison.

Metzger MJ, Bunce RGH, Jongman RHG et al. (2012) A high-resolution bioclimate map of the world: a unifying framework for global biodiversity research and monitoring. *Global Ecology and Biogeography*, 22, 630-638.

Thanks for the relevant reference, it has been cited in the revised manuscript. However, as we mentioned above, by using our approach we really aim for detecting regions of consistent behavior in response to climate (based on the learned weights). That is what we should evaluate. As such, we cannot really aim for ‘accurate’ biomes. This

is the reason why we do not compare our result to other data-driven approaches described in our introductory section that rely on climate and/or vegetation data (as Metzger et al. (2012)); our study tries to detect regions based on different criteria (based on the interaction between climate–vegetation and not on the data). This difference has been also stressed in the revised manuscript. We also note again that the comparison that is provided against traditional land classification schemes is to assure that comparable regions arise from our data-guided approach, despite these land cover types not being explicitly prescribed. See also our answer to the remark 1.3 for the comparison of PCA-based methods to the proposed approach.

p2.11: *Metzger et al. (2012) applied an alternative data-driven approach on climate and vegetation data that used principal component analysis (PCA) to discover informative structures in the data. In this method, the principal components of the initial climate–vegetation data set were applied as input to a clustering algorithm.*

1.8) Figure 4. (c) The Köppen classification divides the world into 5 main classes and 29 sub-classes. The authors should justify the use of 10 classes in the figure. This can be very misleading when looking and interpreting the results. An example: I do not think that the statement p14, l21-23 ‘...the region of North Asia is coherent in terms of climate, but quite diverse in terms of vegetation types; the hydro-climatic biomes show a clear distinction from shrublands (...) to coniferous ...’ holds entirely when looking at the high level details (29 classes) of the Köppen classification. Please justify your choice here.

It is true that the Köppen climate classification scheme consists of divisions and sub-divisions of the five main climate types. We could choose to use the divisions of the Köppen classification, which are basically 12 (if we also divide the tropics further) and not 10 as in Fig. 4. However, the use of 10 instead of 12 classes will not make the map look much different. Moreover, from the color scheme used in Fig. 4, it is clear that there are five main classes. In Fig. 4, we aim for comparing the regions detected by the proposed method to the regions based on the Köppen climate classification scheme. Since the division of 10 climate classes is closer to the number of regions detected by our approach, we choose this number of regions (10) on Köppen’s map. Nonetheless, we agree that the statements mentioned in the comment sound a bit strong, so we modified them in the revised version. Again, the comparison to the Köppen and IGBP maps serves only as a general evaluation or proof of concept for our hydro-climatic biomes map, since in the end such maps are based on a different rationale. This has been clarified in the revised manuscript. We also visualized the distributions of the three classification schemes (Köppen, IGBP, hydro-climatic biomes) with respect to the mean an-

nual precipitation and mean temperature. These scatter plots serve as a kind of “evaluation” for the statement that our hydro-climatic biomes map combines information from both the Köppen and IGBP maps.

p16.12: *For instance, the region of North Asia is quite coherent in terms of climate based on the 10 climate classes shown here (Fig. 4c), but quite diverse in terms of vegetation type (Fig. 4d); the hydro-climatic biomes show a clear distinction in the transition from shrublands (energy-driven) to coniferous forests (energy- and water-driven).*

p16.21: *The comparison to the Köppen-Geiger and IGBP maps serves only as a general evaluation or proof of concept for our hydro-climatic biomes map, since in the end such maps are based on a different rationale, and thus, there is no intent to ‘outperform’ these classification schemes. However, it can be observed in this comparison that the hydro-climatic biomes map in Fig. 4a combine information on climate and vegetation zones by illustrating regions where vegetation similarly interacts with the multi-month dynamics in climatic and environmental conditions. This conclusion is confirmed by the scatter plots in Figs. 4e-g. Figure 4e depicts our hydro-climatic biomes of Fig. 4a in climate space of mean annual temperature against precipitation, while Fig. 4f shows the same but for the Köppen-Geiger climate classes of Fig. 4c. In Fig. 4f, the five climate classes are well-separated, since their definition is based on these two climatic variables. On the other hand, Fig. 4g depicts the same information but for the IGBP map of Fig. 4d. In this figure, savannahs, tropics, and shrublands appear again well clustered. It can be observed that the scatter plot of Fig. 4e clearly lie between the two previous classifications in terms of clustering. Boreal biomes correspond to cold climate classes, the sub-tropical and mid-latitude water-driven biomes correspond to arid regions, while the transitional biomes correspond to the savannas and croplands.*

1.9) Supplementary material S4. The authors indicate that the best-formed clusters are depicted in FigS4a (hence by the hydro-climatic biomes). I find very difficult to make any final judgment of the best “depiction” (/detection) of biomes based on the 2-dimensional graphs provided here.

We improved these figures in the revised manuscript by using the t-SNE method as dimensionality reduction technique.

p5 of Supplement: *See Figs. S5 and S6 of the revised version in the Supplementary material.*

Technical comments

1.10) P5, l14: please add a reference for the statement: ‘...this kind of modelling is becoming more common in climate science...’

This sentence refers to the previously mentioned studies, which are described in the same paragraph, and serves as a conclusion that MTL approaches are used more common recently than in the past in climate science. We added the relevant references in the sentence.

p6.3: *Although this kind of modelling is becoming more common in climate science (i.e., Subbian and Banerjee (2013); McQuade and Monteleoni (2013); Goncalves et al. (2017); Xu et al. (2016)), it has not been combined (to the best of our knowledge) with clustering approaches in the context of mapping land cover nor climate-vegetation dynamics.*

1.11) P10, l10: please clarify what you mean by multi-month vegetation dynamics. Is it seasonal, subseasonal, yearly?

We replaced “multi-month” with “mean monthly” vegetation dynamics.

1.12) P12, l5: please correct ‘Geanger’ with ‘Granger’

Corrected.

1.13) Figure 4. (a) the color code for the clusters sub-tropical energy driven and mid-latitude temperature driven are too similar. It is difficult to differentiate them. Please adjust the color scheme of the legend.

Adjusted.

1.14) p15, l22: The term ‘turning point’ has only been introduced recently in ecosystem and climate science so for clarity, you can refer to: Horion S, Prishchepov AV, Verbesselt J, De Beurs K, Tagesson T, Fensholt R (2016) Revealing turning points in ecosystem functioning over the Northern Eurasian agricultural frontier. Glob Chang Biol, 22, 2801-2817.

We included this relevant reference in the revised manuscript.

Response to the comments of Referee#2

This study presents a new approach for the classification of global biomes. The idea is to focus on the statistical sensitivities of NDVI anomalies to multiple predictors. I do think that it is important to emphasize the “goal” of classifica-

tion, and therefore the paper is a step in the right direction.

We would like to thank the reviewer for the constructive feedback and thorough assessment. Below we provide a point-by-point response to each comment.

2.1) I have, however, doubts if focusing on NDVI anomalies is the right target. In particular for tropical ecosystems NDVI does not tell us much about ecosystem dynamics and the figures show the underlying predictions are indeed not convincing. Hence, I have some doubts about the novelty that this classification can offer. Similar as all classical approaches, also this method fails to reveal the complex spatial patterns in tropical ecosystems. This is why I see this paper more as a methodological contribution that can actually help future studies to realize analogous exercises based on different data sets.

We agree with the reviewer that although NDVI is a commonly-used index, it is known to saturate in tropical ecosystems. As we discussed in our previous work (Papagiannopoulou et al., 2017), the low predictive power of our model in tropical regions can be explained by the fact that in these regions, (i) the uncertainty in the data is larger, and (ii) vegetation might be primarily affected by other factors such as nutrient availability (rather than climate). However, with the proposed data-driven framework, pixels that belong to these tropical regions are grouped together. This means that the learned weight vectors of these pixels are similar and thus the clustering algorithm is able to detect these similarities to conform a coherent biome. Moreover, we also agree that our work can be seen as a methodological contribution, since it can be used in different application scenarios or with an alternative target variable. So, we are willing to explore the applicability of the method to a different target variable. As such, the applicability to microwave Vegetation Optical Depth (VOD) anomalies, instead of the NDVI anomalies, has been explored, see Fig. S7 in the Supplementary material. The result is quite close to the one in the manuscript (Fig.4a) (with the NDVI anomalies as target variable).

p17.8:Results for microwave vegetation optical depth (VOD) (Liu et al., 2011) anomalies as alternative to NDVI anomalies are consistent as shown in Supplementary material Fig. S7.

2.2) Overall, the approach of the paper is to stack a series of methods. First, “Multi-Task Learning” is used to create a statistical prediction model whose sensitivities (condensed by SVD) later serve as basis for clustering. I applaud the authors for identifying a machine learning method that seems to capture spatial relationships. But my question is if there is no corresponding geostatistical approach out there that could be equally used (e.g. a GWR or so) which deals exactly with such questions? In particular, I believe (but don’t know) that

the MTL does not consider the fact that lat-lon grid cells represent different geographical distances, or how do the authors considered that a global analysis is executed on a sphere?

As we have described in the manuscript, our approach is purely data-driven. Therefore, we stress that we do not include any prior knowledge about the distances between the different pixels. On the contrary, we let the method learn the relationships between the different pixels. As such, the method may even group together remote pixels in which vegetation might have similar response to climate. Other geostatistical approaches, such as the GWR, assume that neighboring pixels have a similar behaviour with respect to specific variables. In these approaches, similarities between the pixels are learned by defining each time a single pixel as centroid and tuning the parameter of relatedness between this particular pixel and the surrounding pixels. In our work, we prefer to avoid this kind of neighborhood assumptions and focus on the discovery of relationships between the pixels based on the similarity in climate-vegetation interaction. We are also interested in methods that can be applied on large data sets with global coverage. However, we included this kind of methods as relevant work in the introduction of the revised manuscript.

p2.23: *Previous studies rely on spectral information, supervised techniques or clustering approaches, which are applied to observations of climate variables and/or vegetation characteristics. However, these classification schemes are not based on the type of response of vegetation to climate dynamics. Recent advances in understanding vegetation response to climate variability highlight the importance of revealing the sensitivity of ecosystems to climate conditions, see Nemani et al. (2003); De Keersmaecker et al. (2015); Seddon et al. (2016); Papagiannopoulou et al. (2017b); Liu et al. (2018). Therefore, a step beyond these previous studies is a spatial characterization of the vegetation dynamics that are induced by climate variability, so that ecosystems of similar response to climate anomalies can be unveiled. This objective could be tackled by geostatistical approaches, such as geographically weighted regression (GWR) (Brunsdon et al., 1996), which assume that neighboring pixels have a similar behaviour with respect to specific variables; these methods have already been applied in studies with a regional focus (Propastin et al., 2008; Zhao et al., 2015; Georganos et al., 2017).*

2.3) The paper is neatly written, but I still had trouble finding my way through the paper. One aspect is that it is difficult to follow the paper without knowing the authors previous papers. In addition, I spent most of my time understanding Multi Task Learning. In particular section 2.4. was hard to understand. At this crucial point I would ask the authors to consider rewriting the paper in a

way that can be understood intuitively by environmental scientists who are not familiar with the method. Likewise the link to clustering is a bit opaque. What is a “hierarchical agglomerative clustering approach”? Etc.

We expanded Section 2.4 to make the method more intuitive for the broad audience of GMD. Specifically, we provided additional explanations for the notation used in our model. For the clustering technique that we used, see our answer to remark 1.4.

p9.9: *To clarify the notation used in the ASO method, we intuitively explain the symbolization of the method in relation to our specific setting; the problem of detecting locations with similar climate–vegetation dynamics. As mentioned above (Sect. 2.2 and 2.3), the input features that constitute the $\mathbf{X}^{(l)} \in \mathbb{R}^{N \times d}$ matrix consist of the climatic predictor variables, i.e., the extreme indices, lagged variables, etc., calculated based on raw climatic time series of a certain location l . The dimensions N and d correspond to the number of observations, i.e., the length of the time series and the number of predictor variables, respectively. The target variable for a particular location l , which is the NDVI anomalies, is symbolized with $\mathbf{y}^{(l)} \in \mathbb{R}^N$. As such, an observation of a certain location l at a particular timestamp i is denoted as a pair $(\mathbf{x}_i^{(l)}, y_i^{(l)})$. The goal of the ASO method is to learn the weight matrix $[\mathbf{w}^{(1)}, \mathbf{w}^{(2)}, \dots, \mathbf{w}^{(L)}]$, i.e., a single weight vector $\mathbf{w}^{(l)}$ for each location l . This weight vector $\mathbf{w}^{(l)}$ is able to capture the relationship between the predictor variables and the target, i.e., the climatic variables and the NDVI anomalies. Therefore, climatic predictors that are more important for vegetation anomalies correspond to higher absolute values in the weight vector $\mathbf{w}^{(l)}$. As a result, locations with similar weights are considered as regions where vegetation responds to climate in a similar way. As described in a previous paragraph of this section, the ASO method assumes that the weight vectors $\mathbf{w}^{(l)}$ consist of two parts the $\mathbf{u}^{(l)}$ and the $\mathbf{v}^{(l)}\Theta$. These two parts are learned simultaneously in Algorithm 1 in an alternating fashion. The first part, i.e., the $\mathbf{u}^{(l)} \in \mathbb{R}^d$ belongs to the high-dimensional space, the initial one, which is equal to d . This part expresses the location-specific part of the weight vector, i.e., the deviation of each location’s weight vector from the weights learned in a lower dimensional space. The second part consists of the matrix $\Theta \in \mathbb{R}^{h \times d}$ that represents the map from the initial dimension d to the lower dimension h and the weight vector $\mathbf{v}^{(l)} \in \mathbb{R}^h$. The map matrix Θ is common for all the locations (tasks) and can be learned across them due to the MTL approach. The weight vector $\mathbf{v}^{(l)}$ represents the projection of the initial weights to a low-dimensional space h . Intuitively, this second part of the weight decomposition expresses the coarsest and most important part of weights, since it detects the most important structures through the*

map matrix Θ . The matrix $V = [v^{(1)}, \dots, v^{(L)}]^T \in \mathbb{R}^{L \times h}$ denotes the representation of the models in the low-dimensional space h for the L locations.

2.4) What irritated me about the results is that the prediction method does not manage to explain more than 40% of the variance (why else would the scale in Fig. 3 a otherwise be cut off at ≥ 0.4 ?). This is actually a bit disappointing and suggests that the regression model was not the right choice, or?

In our study, the seasonal cycle from the NDVI time series is removed. Therefore, the task of predicting the NDVI anomalies is more difficult than just predicting the raw NDVI time series. This is due to the fact that the presence of autocorrelation in the NDVI anomalies time series is much lower. Note that if we target the raw NDVI time series (which includes the seasonal component), the R^2 is close to 1 in most of the regions (Papagiannopoulou et al., 2017). In addition, it is worth noting that there are other factors – such as fires, harvesting, etc. – that affect vegetation dynamics but are not included in the data set. Therefore, we should be aware that we focus on explaining the variance of the NDVI anomalies, taking into account only climatic variables.

Minor remarks:

2.5) The introduction does not provide a systematic overview of alternative approaches. Rather, we find here a rather random selection of climate and land cover classifications and the wording is not always correct. For example, the paper speaks of “big data” approaches, but I did not find any of the referenced studies really dealing with big data topics (“volume”, “diversity”, “speed”, ...). I think we are talking here about (sometimes semi-heuristic), but essentially classical data exploration and machine learning methods. So, I think it would be nice to revise this part a bit to have a smooth start.

In general, we would like to stress that the goal of our study is to provide a new data-driven methodology that can identify coherent regions in which vegetation responds to climate in a similar way. To the best of our knowledge, there are no other works that study this particular problem at global scale, with the arguable exception of the article pointed to by Referee#1 (Ivits et al., 2014). In addition, in the manuscript, we describe the most naive approach that one could follow by using single-task learning techniques (and by learning one model per pixel). In the Introduction, we provide an overview of the most related works to our study that indeed use machine learning methods and/or prior knowledge. We think that our work builds upon and goes one step further from previous efforts, such as the ones described in the Introduction, since it combines information

from climate and vegetation and models the relationship between them. However, we added some relevant literature in the introductory section, see our answers to remarks 1.2 and 2.2. In addition, the term “big-data” has been replaced by “data-driven” in the revised manuscript.

p2.7: *As such, data-driven methods have become popular in their use for land cover and climate classifications.*

2.6) The paper is full of shortcuts such as “detrended seasonal NDVI anomalies”, which are not as clear as they appear at first glance. I can think of a large number of possibilities for robustly estimating (linear/non-linear) trends and a further variety of methods for estimating seasonal cycles. It would be nice if such statements were more precise.

We agree that these terms are not clearly described in the manuscript, and understand that the article should stand alone without the need of prior knowledge with regards to our previous work. We added additional statements to briefly describe this terminology in the revised manuscript.

p3.28: *The target variable of our machine-learning framework is the de-trended seasonal NDVI anomalies. These are calculated through a simple linear de-trending and a multi-year average for each month of the year to capture the seasonal expectation see Papagiannopoulou et al. (2017a) for more details. All other data sets, describing the multi-month local climate variability over the three-decade period, are used as predictor variables.*

In addition, a wide range of ‘high-level features’ have been hand-crafted from the raw time series of predictors, and used as well as predictor variables. As such, our set of predictive features includes not just the raw data time series of each climate/environmental variable, but also: seasonal anomalies, de-trended seasonal anomalies, lagged variables, past cumulative variables, and extreme indices see Papagiannopoulou et al. (2017a). The cumulative variables capture the climatic conditions up to present time; an example would be the precipitation of the last (e.g.) three months. Extreme indices include maximum/minimum values, consecutive dry days, values for specific percentiles, etc.

2.7) The same comment applies to the selection of predictors e.g. seasonal anomalies, detrended seasonal anomalies, time delayed variables, and cumulative variables etc. look like a very arbitrary selection of predictors. In a paper that has a strong affinity to data-driven methods, I would expect a more formal variable selection following a clearly defined cost function. Maybe this is too late now, but still one question can be answered: why are these predictors all

regarded as “non-linear”? In most cases, they read like fairly linear transformations (maybe with the exception of cumulative variables).

We refer the reviewer to our previous answer (2.6) for the first part of the comment. In addition, we would like to stress that our choice to use this set of predictors is based on the previous literature, as it has been analytically described in Papagiannopoulou et al. (2017). The constructed predictors are regarded as “non-linear”, because their derivation from the raw data is not linear (see e.g. calculation of extreme indices). This has also been clarified in the revised manuscript.

p4.4: *The use of these non-linear features (non-linear due to the way that have been calculated) greatly improves causal inference and helps characterise non-linear relationships between climate and vegetation dynamics, as shown in our recent work (Papagiannopoulou et al., 2017a).*

References

Papagiannopoulou, C., Miralles, D. G., Decubber, S., Demuzere, M., Verhoest, N. E. C., Dorigo, W. A., and Waegeman, W. A non-linear Granger-causality framework to investigate climate-vegetation dynamics, *Geosci. Model Dev.*, 2017, 10, 1945-1960

Ivits, E., Horion, S., Fensholt, R., Cherlet, M. Global Ecosystem Response Types Derived from the Standardized Precipitation Evapotranspiration Index and FPAR3g Series. *Remote Sensing*, 2014, 6, 4266-4288.

Zhao, Z., et al. Exploring spatially variable relationships between NDVI and climatic factors in a transition zone using geographically weighted regression. *Theoretical and Applied Climatology* 120.3-4, 2015, 507-519.

Demšar, J. Statistical comparisons of classifiers over multiple data sets. *Journal of Machine learning research*. 2006, 7(Jan), 1-30.

Diebold, F. X. Comparing predictive accuracy, twenty years later: A personal perspective on the use and abuse of Diebold-Mariano tests. 2015, *J. Bus. Econ. Stat.*, 33.

Papagiannopoulou, C., Miralles, D. G., Dorigo, W. A., Verhoest, N. E. C., Depoorter, M., and Waegeman, W. Vegetation anomalies caused by antecedent precipitation in most of the world, *Environ. Res. Lett.*, 2017, doi:10.1088/1748-9326/aa7145.

Metzger, M. J., Bunce, R. G. H., Jongman, R. H. G. et al. A high-resolution bioclimate map of the world: a unifying framework for global biodiversity re-

search and monitoring. *Global Ecology and Biogeography*, 2012, 22, 630-638.

Global hydro-climatic biomes identified via multi-task learning

Christina Papagiannopoulou¹, Diego G. Miralles², Matthias Demuzere², Niko E. C. Verhoest², and Willem Waegeman¹

¹Department of Data Analysis and Mathematical Modelling, Ghent University, Belgium,

²Laboratory of Hydrology and Water Management, Ghent University, Belgium

Correspondence: Christina Papagiannopoulou (christina.papagiannopoulou@ugent.be)

Abstract. The most widely-used global land cover and climate classifications are based on vegetation characteristics and/or climatic conditions derived from observational data. However, these classification schemes do not directly stem from the characteristic interaction between the local climate and the biotic environment. In this work, we model the dynamic interplay between vegetation and local climate in order to delineate ecoregions that share a coherent response to hydro-climate variability. Our novel framework is based on a multi-task learning approach that discovers the spatial relationships among different locations by learning a low-dimensional representation of predictive structures. This low-dimensional representation is combined with a clustering algorithm that yields a classification of biomes with coherent behaviour. Experimental results using global observation-based data sets indicate that, without the need to prescribe any land cover information, ~~our method is able to identify~~ the identified regions of coherent climate-vegetation interactions ~~that~~ agree well with the expectations derived from traditional global land cover maps. The resulting global ‘hydro-climatic biomes’ can be used to analyse the anomalous behaviour of specific ecosystems in response to climate extremes and to benchmark climate-vegetation interactions in Earth system models.

1 Introduction

Approaches which aim to define regions with similar biophysical characteristics are commonly known as land cover classification schemes, and are widely used in multiple geoscientific disciplines. Land cover classifications are crucial to enable a better understanding of the spatial variability of the land surface, which can be a first and necessary step towards understanding complex spatio-temporal interactions among different environmental variables (Feddema et al., 2005). Traditional land use/land cover (change) classifications are typically based on spectral information from the land-surface coming from satellites (Loveland and Belward, 1997; Congalton et al., 2014). Amongst the most well-known and widely used are the International Geosphere-Biosphere Program DISCover Global 1km Land Cover classification (IGBP-DIS) (Loveland et al., 2000), Global Land Cover 2000 (Bartholomé and Belward, 2005) and more recently the land cover map developed within the European Space Agency’s Climate Change Initiative (ESA CCI) (Poulter et al., 2015; Li et al., 2018). Similarly, climate classification schemes cluster regions with similar climate conditions and are also widely used to stratify geographical regions with different climatic expectations (Baker et al., 2009; Brugger and Rubel, 2013; Garcia et al., 2014; Herrando-Pérez et al., 2014). Here, the ~~most well-known~~ best known is probably the ~~one from Köppen (1936), the~~ Köppen-Geiger climate classification (Köppen, 1936).

which has been modified many times in recent decades (e.g. Thornthwaite, 1943; Trewartha and Horn, 1980; Feddema, 2005; Kottek et al., 2006; Peel et al., 2007). Yet to date, dynamics in these climate regimes are used as ~~a~~ diagnostic of climate change by exploring their shifting boundaries (e.g. Diaz and Eischeid, 2007; Chen and Chen, 2013; Zhang and Yan, 2014a, b; Spinoni et al., 2015; Chan and Wu, 2015) or as a means to predict future climatic zone distributions ~~based on climate model data~~ using climate projections (e.g. Hanf et al., 2012; Gallardo et al., 2013; Mahlstein et al., 2013).

In recent years, the exponential advance in Earth observation research has made climate science one of the most data-rich scientific domains (Faghmous and Kumar, 2014). As such, ~~big-data~~ data-driven methods have become popular in their use for land cover and climate classifications. For instance, Lund and Li (2009) proposed a new distance measure to define seasonal means and autocorrelations of climatic time series from weather stations, and grouped the stations using a hierarchical agglomerative clustering. Zscheischler et al. (2012) also stressed the importance of ~~the~~ unsupervised methods for tasks such as the classification of the land surface into zones with different climate and vegetation characteristics. Metzger et al. (2012) applied an alternative data-driven approach on climate and vegetation data that used principal component analysis (PCA) to discover informative structures in the data. In this method, the principal components of the initial climate-vegetation data set were applied as input to a clustering algorithm. Interesting results in the same direction can be attributed to Netzel and Stepinski (2016, 2017), who used distance measures of climatic variables, such as dynamic time warping, coming from the time series analysis in a data mining approach. In addition, temporal change in climate zones has been explored in the same context via clustering algorithms, such as k-means (Zhang and Yan, 2014a, b). Finally, data-driven methods have been also applied for the biome classification task, which has been commonly treated as an object recognition problem using remote sensing data. In this case, techniques coming from computer vision are frequently applied (Mekhalfi et al., 2015; Chen and Tian, 2015). Following the progress in computer science, neural networks and deep learning approaches are also becoming popular for this kind of tasks in recent years, making the whole procedure even more automated (Scott et al., 2017; Xu et al., 2018).

~~All the previous~~ Previous studies rely on spectral information, supervised techniques or clustering approaches, which are applied to observations of climate variables and/or vegetation characteristics. However, these classification schemes are not based on the type of response of vegetation to climate dynamics. Recent advances in understanding vegetation response to climate variability highlight the importance of revealing the sensitivity of ecosystems to climate conditions, see Nemani et al. (2003); De Keersmaecker et al. (2012); and Zhang et al. (2015). Therefore, a step beyond these previous studies is a spatial characterization of the vegetation dynamics that are induced by climate variability, so that ecosystems of similar response to climate anomalies can be unveiled. This objective could be tackled by geostatistical approaches, such as geographically weighted regression (GWR) (Brunsdon et al., 1996), which assume that neighboring pixels have a similar behaviour with respect to specific variables; these methods have already been applied in studies with a regional focus (Propastin et al., 2008; Zhao et al., 2015; Georganos et al., 2017). However, here, we aim to avoid neighborhood assumptions and focus on the discovery of relationships between pixels based on the similarity in their modelled climate-vegetation interaction, acknowledging that global ecosystems may experience similar interactions even if they are remotely located from each other. A previous effort towards detecting regions with similar vegetation response to climate

involves the work of Ivits et al. (2014), where PCA is performed on the data matrix of drought anomalies and vegetation state, and a clustering is applied to the correlation coefficients based on the spatio-temporal patterns obtained by PCA. However, in this study, the interaction between climate and vegetation is not explicitly learned, nor the causes behind vegetation changes are inferred in a predictor–target framework.

5 Here, we introduce for the first time (to the best of our knowledge) a data-driven approach that aims to quantify the response of vegetation to local climate variables in a supervised setting at a global scale, and use this information to define ecoregions of consistent behaviour against hydro-climatic ~~conditions. In other words, the emerging regions are areas~~ variability. In simple terms, our framework results in regions where vegetation responds similarly to the dynamics in temperature, soil moisture, incoming radiation, etc. The proposed framework relies on predictive modelling and clustering techniques and builds further
10 upon recent work in which we investigated the global response of vegetation to ~~climate for each global 1-degree pixel separately by applying a machine learning algorithm~~ local climate by applying machine learning algorithms in a Granger causality setting (Papagiannopoulou et al., 2017a, b). Since here we aim to exploit the relationships ~~from different pixels, between different pixels – instead of modelling each pixel separately as in our previous work –~~ we propose the use of multi-task learning (MTL) methods (Caruana, 1997). These methods are commonly used for solving multiple related tasks: considering as one task the pre-
15 diction of vegetation in one location and as multiple tasks the prediction of vegetation in multiple locations, we can model our problem by using an MTL approach. ~~As such, we first~~ First, we apply an MTL approach which tries to unveil low-dimensional common predictive structures and exploit the ~~relation~~ relationships among them. Second, we employ a clustering technique on these informative structures ~~which are constructed using the MTL approach, which is applied on a lower-dimensional space~~ (Sect. 2). This clustering technique is ~~applied on a lower-dimensional space, yielding robust results; this~~ known as spectral
20 clustering (Ng et al., 2002), and is one of the core assets of ~~the method which is known as spectral clustering (Ng et al., 2002)~~ our framework. We refer to ~~these coherent vegetation-climate regions~~ the emergent regions of coherent vegetation-climate behaviour as *hydro-climatic biomes* (Sect. 3).

2 Methodology

2.1 Data sets

25 We have built a large database of global climate and vegetation data that will be used in the context of our framework. These data are described in detail in Papagiannopoulou et al. (2017a) and are mostly based on satellite and/or *in situ* observations. The database spans a 30-year period (1981-2010) at monthly temporal resolution and 1° latitude-longitude spatial resolution. The most important climatic and environmental drivers of vegetation are included ~~in this database~~, namely: (i) land surface temperature, (ii) near-surface air temperature, (iii) longwave/shortwave surface radiative fluxes, (iv) precipitation, (v) snow
30 water equivalent, and (vi) soil moisture. To characterise vegetation, we use the Global Inventory ~~Modeling~~ Modelling and Mapping Studies (GIMMS) NDVI 3g data set (Tucker et al., 2005). The target variable of our machine-learning framework is the de-trended seasonal NDVI anomalies ~~calculated as in Papagiannopoulou et al. (2017a), while all~~. These are calculated through a simple linear de-trending and a multi-year average for each month of the year to capture the seasonal expectation –

see Papagiannopoulou et al. (2017a) for more details. All other data sets, describing the multi-month local climate variability over the three-decade period, are used as predictor variables.

In addition, a series-wide range of ‘high-level features’ have been hand-crafted from the raw time series of predictors, and used as well as predictor variables. As such, our set of predictive features includes not just the raw data time series of each climate/environmental variable, but also: seasonal anomalies, de-trended seasonal anomalies, lagged variables, past cumulative variables, and extreme indices — see Papagiannopoulou et al. (2017a). The cumulative variables capture the climatic conditions up to present time; an example would be the precipitation of the last (e.g.) three months. Extreme indices include maximum/minimum values, consecutive dry days, values for specific percentiles, etc. The use of these non-linear features greatly-improved (non-linear due to the way that have been calculated) greatly improves causal inference and help-helps characterise non-linear relationships between climate and vegetation dynamics, as shown in our recent work (Papagiannopoulou et al., 2017a). For a further discussion about the importance of the-this higher-level feature representation adopted in our framework, we refer the reader to Sect. S1 of the Supplementary material.

2.2 Pixel-based approach: single-task learning

In our study, we use information on climate and vegetation variables at specific time points and locations. Formally, we consider a spatio-temporal data set $D = \{(\mathbf{X}^{(1)}, \mathbf{y}^{(1)}), (\mathbf{X}^{(2)}, \mathbf{y}^{(2)}), \dots, (\mathbf{X}^{(L)}, \mathbf{y}^{(L)})\}$, with L being the number of different locations and $(\mathbf{X}^{(l)}, \mathbf{y}^{(l)})$ the tuple of the predictor variables and the target variable of each location l . We denote $D^{(l)} = \{(x_i^{(l)}, y_i^{(l)})\}_{i=1, \dots, N}$ the observations of a location l while the input feature vectors (i.e. the set of climatic variables) are denoted as a matrix $\mathbf{X}^{(l)} = [x_1^{(l)}, \dots, x_N^{(l)}]^T$ and the corresponding target values as $\mathbf{y}^{(l)} = [y_1^{(l)}, \dots, y_N^{(l)}]^T$ (i.e., the NDVI anomalies). Specifically, $\mathbf{X}^{(l)} \in \mathbb{R}^{N \times d}$ is the matrix of the predictor variables with d being the number of predictors, and $\mathbf{y}^{(l)} \in \mathbb{R}^N$ the response time series (i.e., NDVI seasonal de-trended anomalies), where N denotes the number of discrete time stamps, i.e., the length of the time series. In this setting, a straightforward approach is to tackle each regression problem in each location l separately, i.e., by independently training one model for each location (Papagiannopoulou et al., 2017a). That way, for every pixel only the data of that particular location l is used $((\mathbf{X}^{(l)}, \mathbf{y}^{(l)}), l = 1, \dots, L)$, not attempting to utilize the data from other regions where the target variable might have a similar response to the predictors. As such, we can start by defining regions of similar climate-vegetation dynamics with the most naive approach: the relationship between climate and vegetation can be caught by the weights of a simple regression model, i.e., the regression coefficients of the predictor variables. Specifically, if one defines a simple linear regression model for a location l , the model for the l th location is given by $f^{(l)}(x_i^{(l)}) = w^{(l)} x_i^{(l)}$, with $x_i^{(l)}$ being the input data (i.e., one observation) and $w^{(l)}$ being the weight vector learned for particular location l , which describes the importance of each input variable for the target – see Fig. 1a. Even though one can assume that these weight vectors can be similar for regions in which the response of vegetation to climate is similar, the information from these other regions is not used in the prediction (i.e. each regression is applied at each individual pixel separately). This is despite the fact that these locations could be subsequently grouped (e.g., based on a similarity measure of their weight vectors) into wider regions of particular climate-vegetation dynamics, i.e., regions in which vegetation responds to climate in a similar way. Note that one may assume that share common climate-vegetation dynamics.

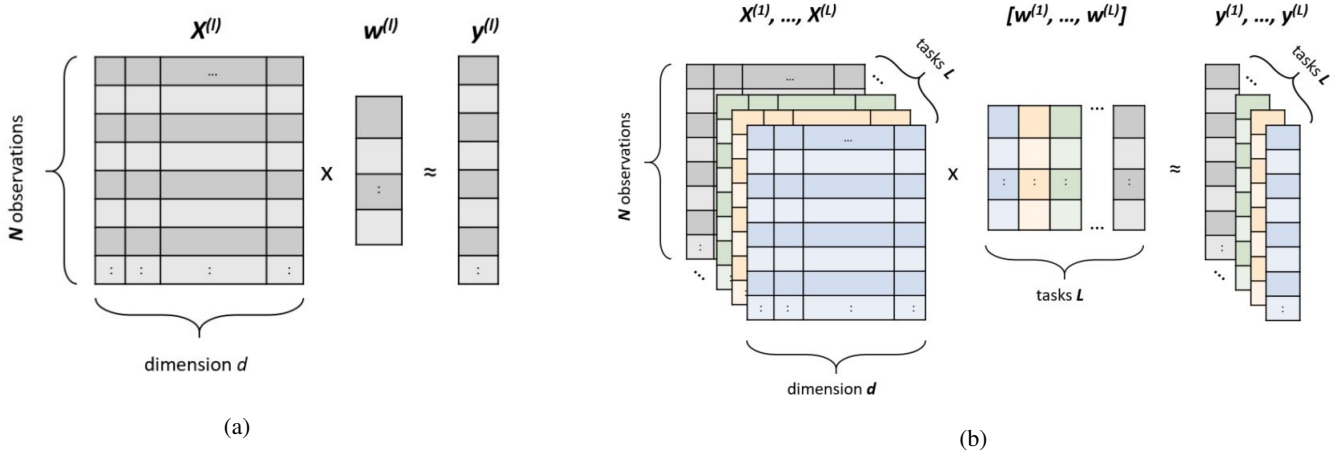


Figure 1. Graphical representation of two learning approaches. (a) A single-task learning approach in which each pixel is treated separately. For each pixel l there is an input data set $\mathbf{X}^{(l)} \in \mathbb{R}^{N \times d}$, with N being the number of observations and d being the number of predictors, and a target vector $\mathbf{y}^{(l)} \in \mathbb{R}^N$. The vector $\mathbf{w}^{(l)} \in \mathbb{R}^d$ represents the weight vector learned by the model. (b) A multi-task learning approach in which the models of L tasks are simultaneously learned. The input of the method is the data sets $\mathbf{X}^{(1)}, \mathbf{X}^{(2)}, \dots, \mathbf{X}^{(L)}$ of all locations (i.e., all global land pixels). The corresponding target vectors are denoted with $\mathbf{y}^{(1)}, \mathbf{y}^{(2)}, \dots, \mathbf{y}^{(L)}$. The weight matrix $[\mathbf{w}^{(1)}, \mathbf{w}^{(2)}, \dots, \mathbf{w}^{(L)}] \in \mathbb{R}^{d \times L}$ contains the weight vectors for all tasks.

[Note also](#) that the information captured by each weight vector $\mathbf{w}^{(l)}$ should be sufficient which means that it is necessary for the models to have a good generalization performance.

2.3 Exploiting spatial relationships: multi-task learning

5 Unlike [the](#) single-task learning models [described above](#), that only take the data of each particular location into account, ~~in-MTL the model has access to shared~~ [MTL models extract](#) information of data sets with similar characteristics from other locations. As such, ~~it~~ [they](#) can be expected to generalize better and give a ~~high~~ [higher](#) predictive performance on unseen data. Specifically, by using the MTL approach, the generalization of the model improves if the dataset of each task is expanded by observations from highly related tasks. This is crucial, especially in cases where the number of training instances per task is limited. The

10 basic idea that underlines the MTL modelling approach is the learning of a separate model for each task and not a unique model trained on a concatenated set of observations of all tasks. Note that in our spatio-temporal data sets, each location can be seen as a different task, and that neighbouring (or distant) locations with similar ~~climate-vegetation~~ [climate-vegetation](#) interactions will tend to have similar (yet not identical) behaviour. In light of this observation, MTL seems to be a quite natural modelling approach to explore the interaction between climate and vegetation in different locations.

15 The idea of MTL is not new (Baxter, 1997; Caruana, 1997; Baxter et al., 2000), and it has been applied in many machine-learning applications in medical sciences (Bi et al., 2008; Zhang et al., 2012) and computer vision (Zhang et al., 2014). It has also been used in climate science to improve the way multiple Earth System Models (ESMs) outputs are combined,

by treating the locations as different tasks (Subbian and Banerjee, 2013; McQuade and Monteleoni, 2013). In these studies, the idea is that in neighbouring locations (pixels which are close to each other), similar ESMs tend to have similar performance (Subbian and Banerjee, 2013; McQuade and Monteleoni, 2013). A recent study proposed a hierarchy of tasks, in which at a first level, tasks of each location are trained into an MTL setting, while at a second level, tasks of each variable are sharing information (Gonçalves et al., 2017). In addition, for modelling spatio-temporal data, Xu et al. (2016) introduced an MTL framework in which local models share a common representation based on the spatial autocorrelation. Although this kind of modelling is becoming more common in climate science (i.e., Subbian and Banerjee (2013); McQuade and Monteleoni (2013); Gonçalves et al. (2017)), it has not been combined (to the best of our knowledge) with clustering approaches in the context of mapping land cover nor climate-vegetation dynamics.

In this work, we focus on MTL methods that can discover the relationship between different tasks (locations) and recover strong predictive structures of the vegetation response to climate. These are then used to conform hydro-climatic biomes, i.e., regions of coherent vegetation behaviour with respect to climate variability (see Sect. 3.3). To this end, we use the same notation as before by denoting $\mathbf{X}^{(l)} \in \mathbb{R}^{N \times d}$ as input data matrix of the predictor variables, $\mathbf{y}^{(l)} \in \mathbb{R}^N$ as the target vector for each location l and $\mathbf{w}^{(l)} \in \mathbb{R}^d$ in which each value corresponds to a weight. We define as $[\mathbf{w}^{(1)}, \mathbf{w}^{(2)}, \dots, \mathbf{w}^{(L)}] \in \mathbb{R}^{d \times L}$ the weight matrix of all locations such that the $\mathbf{w}^{(l)}$ vector is the l -th column of the $[\mathbf{w}^{(1)}, \mathbf{w}^{(2)}, \dots, \mathbf{w}^{(L)}]$ matrix — see a graphical representation of the notation in Fig. 1b. Given a loss function \mathcal{L} (e.g., the squared error loss), the multi-task minimization problem is formulated as:

$$\min_{\mathbf{w}^{(1)}, \dots, \mathbf{w}^{(L)}} \sum_{l=1}^L \sum_{i=1}^N \mathcal{L}(\mathbf{w}^{(l)} x_i^{(l)}, y_i^{(l)}) + \Omega(\mathbf{w}^{(1)}, \dots, \mathbf{w}^{(L)}) \quad (1)$$

where $\Omega(\mathbf{w}^{(1)}, \dots, \mathbf{w}^{(L)})$ is a factor which controls the relatedness among the tasks. In our setting, we assume that there is no prior knowledge about the relationship of the tasks (locations) and we aim to apply a method that can discover these relationships.

In literature, there are many MTL methods that are trying to do two things simultaneously: learn a weight matrix $[\mathbf{w}^{(1)}, \mathbf{w}^{(2)}, \dots, \mathbf{w}^{(L)}]$ and another matrix which captures the task relationships simultaneously (Ando and Zhang, 2005; Chen et al., 2009; Zhou et al., 2011). In real applications, there are scenarios where the tasks of an MTL problem follow a specific structure, i.e., some tasks are more related whereas some others are unrelated. In order to identify this group structure, researchers have developed various methods which have been referred to as clustered multi-task learning (CMTL) methods (Zhou et al., 2011). For instance, Xue et al. (2007) proposed a method which uses a Dirichlet process-based statistical model to identify similarities between related tasks, while Jacob et al. (2009) introduced a framework which identifies groups of tasks and performs the learning at once. In the same direction, Wang et al. (2009) used an inter-task regularization term to take into consideration tasks which have been grouped in the same cluster in a semi-supervised setting. More recently, Barzilai and Crammer (2015) suggested a method which assigns explicitly each task to a specific cluster, building a single model for each task by using linear classifiers which are combinations of some basis. An alternative approach has been proposed by Zhou et al. (2011) in which the structure of the task relatedness is unknown and is learned during the training phase. Interestingly, when case-specific

conditions are fulfilled, this method is equivalent to the method by Ando and Zhang (2005), known as the Alternative Structure Optimization (ASO), which belongs to the category of MTL methods that assume the existence of a shared low-dimensional representation among the tasks. The name of the method indicates that an alternating optimization procedure is involved during the learning process since the weight matrix and the matrix which captures the shared low-dimensional representation are learned simultaneously. Typically, in these procedures, the optimization of each part is separately performed while the other part remains fixed. In our work, we apply the ASO method due to its simplicity and the fact that it does not need a lot of iterations to capture the information about the task relatedness that is needed. This is **very important in our application because** **the crucial for our application, since the large** size of the global database we use (Papagiannopoulou et al., 2017a), puts severe limitations to the choice of method. Another aspect is that by learning this low-dimensional representation we can have a visual inspection of the "most predictive common structures" for each region. In the following section we explain in detail the ASO method used in our setting.

2.4 Learning predictive structures from multiple tasks

The ASO algorithm proposed by Ando and Zhang (2005) learns common predictive structures from multiple related tasks that are assumed to share a low-dimensional feature space. Specifically, by applying this method, one learns one model function for each individual task and the learned weight vector is decomposed into two parts: (a) a high-dimensional space, and (b) a shared low-dimensional space based on a feature map learned during the process. This feature map is a matrix which serves as a link between a high-dimensional space and a low-dimensional space. In our case, L predictor functions $\{f^{(l)}\}_{l=1}^L$ are simultaneously learned by exploiting the shared feature space that underlines all tasks. This low-dimensional feature space is expressed in a simple linear form of a low-dimensional feature map Θ across the L tasks. Mathematically, the function $f^{(l)}$ can be written as:

$$f^{(l)}(x) = w^{(l)} x_i^{(l)} = u^{(l)} x_i^{(l)} + v^{(l)} \Theta x_i^{(l)} \quad (2)$$

with $\Theta \in \mathbb{R}^{h \times d}$ being a parameter matrix with orthonormal row vectors, i.e., $\Theta \Theta^T = \mathbf{I}$, where h is the dimensionality of the shared feature space, and $w^{(l)}$, $u^{(l)}$ and $v^{(l)}$ are the weight vectors for the full feature space, the high-dimensional one (initial dimension d), and the shared low-dimensional one (based on the h parameter), respectively. As mentioned before, the ASO method is equivalent to the CMTL method (Zhou et al., 2011), under a specific condition: that the parameter k , which symbolizes the number of clusters in the CMTL approach, is equal to the parameter h of the ASO method. This condition determines the number of clusters that should be used in the clustering phase of our framework, because the objective of ASO is optimized based on the value of the parameter h . We reconsider this **equality equivalence** in Sect. 3.2 where we discuss about the number of clusters that should be identified based on our analysis.

Formally, ASO can be formulated as the following optimization problem:

$$\min_{\{w^{(l)}, v^{(l)}\}, \Theta \Theta^T = \mathbf{I}} \sum_{l=1}^L \left(\sum_{i=1}^N \mathcal{L}(w^{(l)} x_i^{(l)}, y_i^{(l)}) + \lambda^{(l)} \left\| u^{(l)} \right\|_2^2 \right) \quad (3)$$

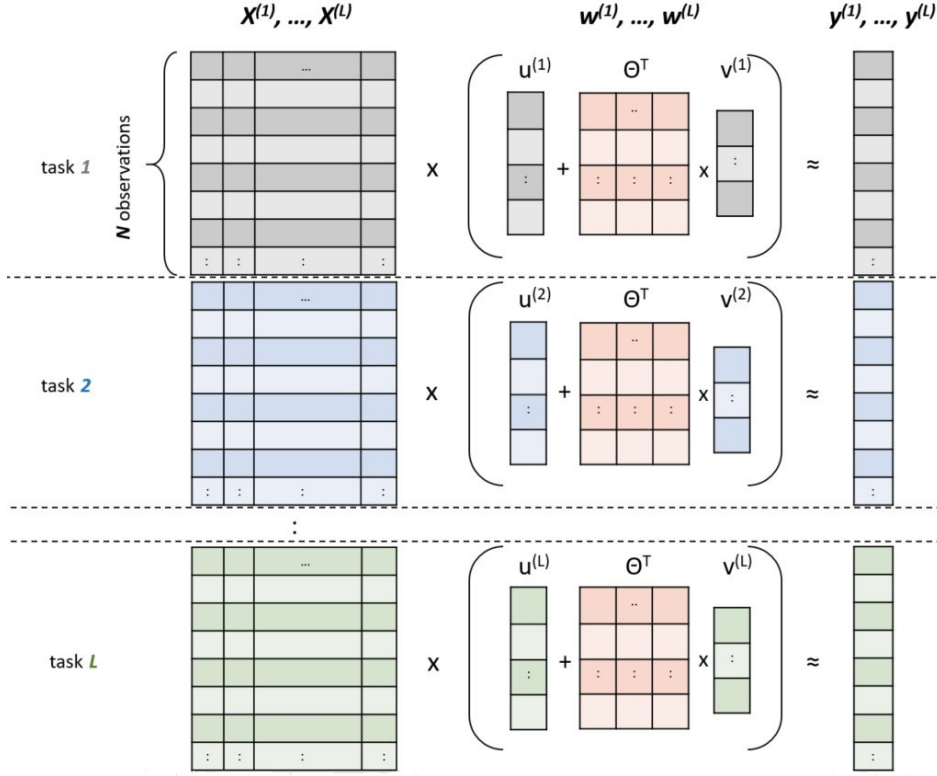


Figure 2. Graphical representation of the ASO method. The input of the method is the data sets $\mathbf{X}^{(1)}, \mathbf{X}^{(2)}, \dots, \mathbf{X}^{(L)}$ of all locations. The corresponding target vectors are denoted with $\mathbf{y}^{(1)}, \mathbf{y}^{(2)}, \dots, \mathbf{y}^{(L)}$. The weight vector $\mathbf{w}^{(l)} \in \mathbb{R}^d$ of the full space is decomposed in two parts; to the weight vector $\mathbf{u}^{(l)} \in \mathbb{R}^d$ of the high-dimensional space and the weight vector $\mathbf{v}^{(l)} \in \mathbb{R}^h$ of the low-dimensional one. The low-dimensional feature map $\Theta^T \in \mathbb{R}^{d \times h}$ is common for all the tasks.

with $\|\mathbf{u}^{(l)}\|_2^2$ being the regularization term ($\mathbf{u}^{(l)} = \mathbf{w}^{(l)} - \Theta^T \mathbf{v}^{(l)}$) ~~which that~~ controls the task relatedness among L tasks, $(\mathbf{x}_i^{(l)}, y_i^{(l)})$ being the input vector and the corresponding target value of the ~~i^{th}~~ ^{i} ~~i^{th}~~ ^{i} observation in a particular location l , and $\lambda^{(l)}$ being a pre-defined parameter – see Fig. 2 for the graphical representation of the notation. During the learning process the weight matrix $[\mathbf{w}^{(1)}, \mathbf{w}^{(2)}, \dots, \mathbf{w}^{(L)}]$ and the matrix Θ , which captures the shared low-dimensional representation, are learned simultaneously. The regularization term $\|\mathbf{u}^{(l)}\|_2^2$, based on the value of the parameter λ , penalizes the differences between the weights on the initial high-dimensional space and the weights on the low-dimensional space parameterized by Θ .

There are several ways of solving the optimization problem ~~of in~~ Eq. (3) (Ando and Zhang, 2005). Our main purpose is to extract the shared feature space ~~$\Theta - \Theta$~~ in order to apply a clustering on the low-dimensional feature space. In this feature space, locations with similar predictive structures will be grouped into the same broader region. For this reason, we adopt the Singular Value Decomposition (SVD)-based ASO algorithm, proposed by Ando and Zhang (2005), which achieves good performance even on the first iteration of the method. As mentioned before, this is crucial to our application given the large number of tasks and the high-dimensional data sets. The steps of the SVD-based ASO are presented in Algorithm 1.

Algorithm 1 SVD-ASO

Input: training data $D^{(l)} = \{(\mathbf{x}_i^{(l)}, y_i^{(l)})\}_{i=1, \dots, N}$, where $l = 1, \dots, L$

Parameters: h and $\boldsymbol{\lambda} = \{\lambda^{(1)}, \dots, \lambda^{(L)}\}$

Output: $\boldsymbol{\Theta} \in \mathbb{R}^{h \times d}$ and $\mathbf{V} = [\mathbf{v}^{(1)}, \dots, \mathbf{v}^{(L)}]^T \in \mathbb{R}^{L \times h}$

Initialize: $\mathbf{w}^{(l)} = 0, l = 1, \dots, L$, and $\boldsymbol{\Theta}$ to random

repeat

for $l = 1$ **to** L **do**

 with fixed $\boldsymbol{\Theta}$ and $\mathbf{v}^{(l)} = \boldsymbol{\Theta} \mathbf{w}^{(l)}$, solve the optimization problem of Eq. (3) for $\mathbf{u}^{(l)}$:

$$\arg \min_{\mathbf{u}^{(l)}} \sum_{i=1}^N \mathcal{L}(\mathbf{u}^{(l)} \mathbf{x}_i^{(l)} + (\mathbf{v}^{(l)} \boldsymbol{\Theta}) \mathbf{x}_i^{(l)}, y_i^{(l)}) + \lambda^{(l)} \|\mathbf{u}^{(l)}\|_2^2) \min_{\mathbf{u}^{(l)}} \sum_{i=1}^N \mathcal{L}(\mathbf{u}^{(l)} \mathbf{x}_i^{(l)} + (\mathbf{v}^{(l)} \boldsymbol{\Theta}) \mathbf{x}_i^{(l)}, y_i^{(l)}) + \lambda^{(l)} \|\mathbf{u}^{(l)}\|_2^2$$

$$\mathbf{w}^{(l)} = \mathbf{u}^{(l)} + \boldsymbol{\Theta}^T \mathbf{v}^{(l)}$$

end for

Apply an SVD decomposition on $\mathbf{W} = [\sqrt{\lambda^{(1)}} \mathbf{w}^{(1)}, \dots, \sqrt{\lambda^{(L)}} \mathbf{w}^{(L)}]$:

$\mathbf{W} = \mathbf{V}_1 \mathbf{D} \mathbf{V}_2^T$ (with diagonals of \mathbf{D} in descending order)

$\boldsymbol{\Theta} = \mathbf{V}_1^T[:, h, :]$ // update $\boldsymbol{\Theta}$ to the first h rows of \mathbf{V}_1^T

until convergence

The SVD-based ASO method can be interpreted as a dimensionality reduction technique applied to the model space (i.e., weights). It should be stressed here that this method must not be confused with ~~principal component analysis (PCA)~~PCA, which is usually employed on the data space (input space of predictors) (Metzger et al., 2012; Ivits et al., 2014). The goal of the ASO method is to detect the principal components of the ~~predictive structures~~parameter matrix, while PCA identifies the principal components of the input data \mathbf{X} . The goal of the ASO method can be achieved by considering the models of multiple tasks as samples of their own distribution. Therefore, these samples can only be formed by using an MTL approach, in which there is access to the models from ~~the~~multiple learning tasks. Moreover, in our work, we explicitly consider the climatic variables as predictors and the vegetation variable as target variable, and we learn the relationship between them in a supervised setting. As such, the regions that we define rely on the relationship between climate and vegetation in a prediction setting, and the clustering is calculated based on similarity of this relationship (i.e. the model coefficients for different locations), see Sect. 2.5 for more details. As such, we learn relationships between climate and vegetation in a supervised setting, whereas PCA-based methods (Metzger et al., 2012; Ivits et al., 2014) are fully unsupervised. In our study the SVD decomposition is used as part of the optimization algorithm, thus in a supervised setting. In this setting, the model weights are optimized based on a given training set. Therefore, the discovered structures are obtained during the training process.

To clarify the notation used in the ASO method, we intuitively explain the symbolization of the method in relation to our specific setting: the problem of detecting locations with similar climate–vegetation dynamics. As mentioned above (Sect. 2.2 and 2.3), the input features that constitute the $\mathbf{X}^{(l)} \in \mathbb{R}^{N \times d}$ matrix consist of the climatic predictor variables, i.e., the extreme indices, lagged variables, etc., calculated based on raw climatic time series of a certain location l . The dimensions N and d correspond to the number of observations, i.e., the length of the time series and the number of predictor variables, respectively.

The target variable for a particular location l , which is the NDVI anomalies, is symbolized with $y^{(l)} \in \mathbb{R}^N$. As such, an observation of a certain location l at a particular timestamp i is denoted as a pair $(x_i^{(l)}, y_i^{(l)})$. The goal of the ASO method is to learn the weight matrix $[w^{(1)}, w^{(2)}, \dots, w^{(L)}]$, i.e., a single weight vector $w^{(l)}$ for each location l . This weight vector $w^{(l)}$ is able to capture the relationship between the predictor variables and the target, i.e., the climatic variables and the NDVI anomalies. Therefore, climatic predictors that are more important for vegetation anomalies correspond to higher absolute values in the weight vector $w^{(l)}$. As a result, locations with similar weights are considered as regions where vegetation responds to climate in a similar way. As described in a previous paragraph of this section, the ASO method assumes that the weight vectors $w^{(l)}$ consist of two parts the $u^{(l)}$ and the $v^{(l)}\Theta$. These two parts are learned simultaneously in Algorithm 1 in an alternating fashion. The first part, i.e., the $u^{(l)} \in \mathbb{R}^d$ belongs to the high-dimensional space, the initial one, which is equal to d . This part expresses the location-specific part of the weight vector, i.e., the deviation of each location’s weight vector from the weights learned in a lower dimensional space. The second part consists of the matrix $\Theta \in \mathbb{R}^{h \times d}$ that represents the map from the initial dimension d to the lower dimension h and the weight vector $v^{(l)} \in \mathbb{R}^h$. The map matrix Θ is common for all the locations (tasks) and can be learned across them due to the MTL approach. The weight vector $v^{(l)}$ represents the projection of the initial weights to a low-dimensional space h . Intuitively, this second part of the weight decomposition expresses the coarsest and most important part of weights, since it detects the most important structures through the map matrix Θ . The matrix $V = [v^{(1)}, \dots, v^{(L)}]^T \in \mathbb{R}^{L \times h}$ denotes the representation of the models in the low-dimensional space h for the L locations.

2.5 Land classification: clustering highly-predictive structures

Clustering in machine learning is the task of grouping a set of samples in such a way that those samples ~~which~~ that belong to the same group (cluster) are more similar with respect to a specific criterion than to samples ~~which~~ that belong to other groups. Clustering techniques are usually based on a distance (or similarity) measure, which is calculated among the samples and/or group of samples. There are several clustering approaches and an in-depth review can be found in Xu and Tian (2015).

It is known that in high-dimensional spaces, the distance measures are not able to capture well the differences between pairs of samples, thus clustering algorithms tend to perform better in lower dimensional spaces. In our setting, we learn the common feature map $\Theta \in \mathbb{R}^{h \times d}$ and the $V = [v^{(1)}, \dots, v^{(L)}]^T \in \mathbb{R}^{L \times h}$ matrix, which is the representation of the models in this low-dimensional space, using the SVD-ASO method – see Sect. 2.4. The V matrix captures the information of the similar predictive structures among all the tasks, so similar tasks are closer in this low dimensional space and as a consequence, they have a similar representation (i.e. ~~similar~~ weights) in this matrix. That way, the clustering techniques based on distance calculations are applied on the more expressive low-dimensional space, resulting in a better performance. As it has been discussed in our previous work (Papagiannopoulou et al., 2017a), global climate-vegetation relationships are complex and non-linear. Here, if the V representation is expressive enough, the clustering method can group together locations with similar models, i.e., locations in which vegetation responds to climate in a similar non-linear way. Thus, it is first necessary to evaluate the quality of the learned matrix V . The most straight forward way to do so, is by measuring the predictive performance of the MTL model in terms of e.g. R^2 . If the predictive power of the model is strong, we can conclude that the V matrix is able to well-capture the relationships of each task with the highly predictive structures. So, given that the V representation is sufficiently learned from

5 the data, we can apply any kind of clustering algorithm on the low-dimensional representation of matrix \mathbf{V} . This approach is also known as spectral clustering due to the fact that the clustering algorithm is applied on a reduced feature space, making the clustering results more robust.

In our application, we use a hierarchical agglomerative clustering approach [\(Ward, 1963\)](#) where the number of clusters is not predefined. In the hierarchical clustering approach, the result is usually depicted as a dendrogram in which the leaves represent the observations and the inner nodes correspond to the data clusters. The dendrogram branches are proportionally long to the value of the intergroup dissimilarity. By defining this hierarchical form of the clustering result, one can define the number of clusters by cutting down vertically (or horizontally, depending on the view) the dendrogram in a point where the dissimilarity between the clusters is high and therefore the branches [are](#) longer – see Sect. 3.2 for the choice of the optimum number of clusters in our analysis.

15 2.6 Experimental setup

In all the experiments, we use as predictors all the climatic data sets and the features that we have constructed from them as well as the 12-lagged values of the target variable. A ~~total-resulting~~ number of 3,209 predictor ~~variables-is-included(climate)~~ [variables is used](#), i.e., $d = 3,209$ in our setting. These variables constitute the input to our framework, i.e., the $\mathbf{X}^{(l)}, l = 1, \dots, L$ data sets. As target variable, we use the NDVI seasonal anomalies [calculated](#) as in Papagiannopoulou et al. (2017a) ~~;~~ [and](#) denoted as $\mathbf{y}^{(l)}, l = 1, \dots, L$ for each location. [For more details about the data sets in our setting see Sect. 2.1.](#) We examine 13,072 land pixels where each pixel constitutes a single task in our MTL setting, i.e., $L = 13,072$. The dataset of each single task consists of 360 monthly observations [given our 30-year study period](#), i.e., $N = 360$. ~~All the methods have been developed in Python.~~

For the STL ~~modeling, modelling, evaluated for comparison,~~ we use the ridge regression for each location independently. Ridge regression is a linear model which uses an ℓ_2 norm regularization term in order to shrink the weight coefficients towards zero ~~to-and~~ avoid over-fitting. In ridge regression the weight coefficients are fitted by solving the following optimization problem:

$$\min_{\mathbf{w}^{(l)}} \sum_{i=1}^N \mathcal{L}(\mathbf{w}^{(l)} \mathbf{x}_i^{(l)}, y_i^{(l)}) + \lambda \|\mathbf{w}^{(l)}\|^2 \quad (4)$$

with λ being a regularization parameter tuned using a separate validation set and $\|\mathbf{w}^{(l)}\|^2$ being a penalty term, i.e., the squared ℓ_2 norm of the weight vector. Note that by splitting the original data set in three parts [\(1\) training set, \(2\) validation set, and \(3\) test set](#) ~~;~~ [we tune the parameters in a set of observations \(validation set\) that are not included in the final test set and that way we have a fair comparison](#) [achieve a fair evaluation](#) of the model ~~performancesperformance~~. The optimization problems of the SVD-ASO algorithm are solved by using the [Limited-memory Broyden-Fletcher-Goldfarb-Shanno \(L-BFGS\)](#) optimization algorithm.

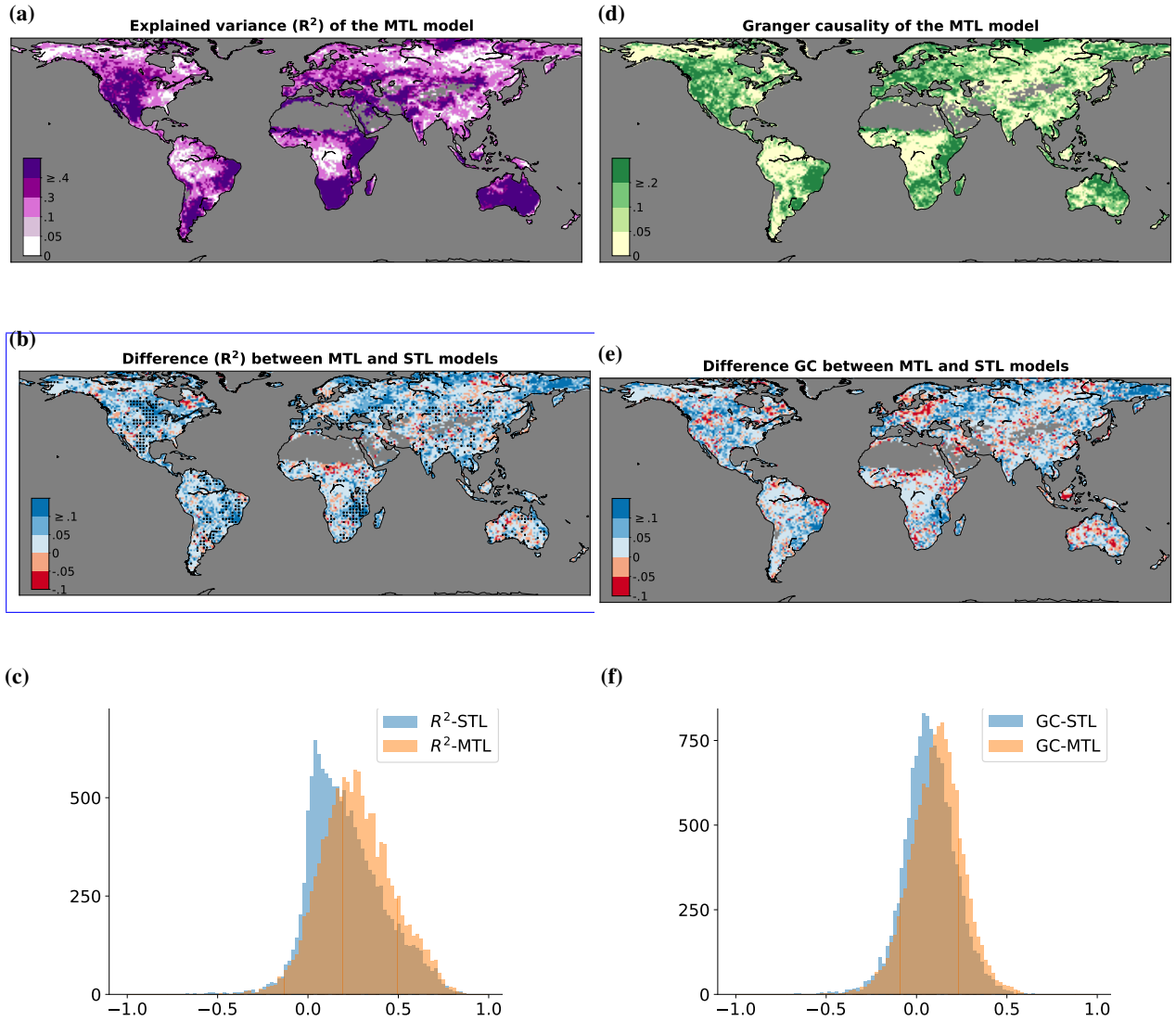


Figure 3. Comparison of the predictive performance between the STL and the MTL approaches. (a) Explained variance (R^2) of the NDVI monthly anomalies based on the MTL approach. (b) Difference in terms of R^2 between the MTL and the STL approaches; blue regions indicate a higher performance by the MTL. The dotted regions correspond to areas where the MTL model significantly outperforms the STL models based on the Diebold-Mariano statistical test (Diebold, 2015). (c) Comparison of the distributions of the R^2 scores in the STL and in the MTL setting; the blue histogram corresponds to the STL, and the orange one to the MTL approach. (d) Quantification of Granger causality for the MTL approach, i.e. improvement in terms of R^2 by the full MTL model with respect to the R^2 of the baseline MTL model that uses only past values of NDVI anomalies as predictors; positive values indicate Granger causality (Papagiannopoulou et al., 2017a). (e) Difference in terms of Granger causality between the MTL and the STL approaches; blue regions indicate a higher performance by the MTL. (f) Comparison of the distributions of the Granger causality in the STL and in the MTL setting; the blue histogram corresponds to the STL, and the orange one to the MTL approach.

3 Results and discussion

5 3.1 Single- versus multi-task learning model

In a first experiment, we compare the predictive performance of the STL model versus the MTL model. For the STL modelling, the ridge regression is used. For the MTL modelling, we apply the ASO-MTL model (Ando and Zhang, 2005) described in Sect. 2. We use a separate validation set to tune the regularization parameter λ for both approaches. For the STL approach, we tune the λ parameter for each location (task) separately, while for the MTL approach we use the same λ value for all the tasks, taking into account the average performance across these tasks. For the ASO-MTL method, we have also experimented with the value of the h parameter, which is the dimensionality of the shared feature space – see Sect. 3.2 for more details about the influence of this parameter on the clustering results. Finally, we evaluate the performance of both approaches in terms of R^2 , as in Papagiannopoulou et al. (2017a). Figure 3 depicts the result of our comparison. Figure 3a shows the R^2 of the ASO-MTL model while Fig. 3b highlights the difference in predictive performance of the MTL model in comparison with the STL model. As shown in Fig. 3b, in almost all regions of the world, the predictive performance increases substantially compared to the STL approach. In fact, over extensive regions (40% of the study area), more than ~~40~~5% of the variability in NDVI is explained by the spatial structure of the data. In statistical terms, this implies the existence of a hidden structure between the different locations (tasks), which is informative with respect to our target variable. The dotted regions in Fig. 3b correspond to areas where the MTL model significantly outperforms the STL models based on the Diebold-Mariano statistical test, which compares model predictions (Diebold, 2015). For the statistical test, we use the False Discovery Rate (Benjamini and Hochberg, 1995) method to correct the p-values at level 0.05 due to the multiple-hypothesis testing setting.

Additionally, Fig. 3a shows that more than 40% of the ~~multi-month-mean monthly~~ vegetation dynamics can be explained by climate variability in some regions. In particular, in regions such as Australia, Africa and Central and North America, the predictive power of the model is stronger in terms of R^2 , following the same pattern and scoring similar R^2 values as the random forest approach by Papagiannopoulou et al. (2017a). To deepen on the performance difference between the two approaches, the R^2 scores are presented as two different distributions in Fig. 3c. The blue histogram corresponds to the distribution of the R^2 scores of the STL approach, while the orange one corresponds to the distribution of the R^2 scores of the MTL approach. As it can be observed, the distribution of the R^2 scores is shifted to the right for the MTL, meaning that values are typically greater than those derived from the STL approach. Moreover, the skew towards the left in the blue histogram, with values close to zero, is an indication of the near-zero performance of the STL models in many locations. The Wilcoxon paired statistical test (Demšar, 2006) confirms that the results of the two approaches are overall statistically different (p-value $< 10^{-9}$).

Since we are ultimately interested in investigating regions of coherent ~~vegetation-climate-interactions~~impact of climate variability on vegetation dynamics, we also evaluate the ability of the MTL model to detect Granger-causal effects of climate on vegetation. For a detailed description of the Granger causality modelling framework we direct the reader to Papagiannopoulou et al. (2017a). This point is crucial to understand the extent to which the climatic predictors carry additional information about the dynamics in vegetation that is not contained in the past vegetation signal itself. The results of applying the Granger causality analysis using MTL modelling are shown in Figure 3d, which illustrates results of the full MTL model compared to the baseline

MTL model. This baseline model only uses previous values of NDVI to predict monthly NDVI anomalies (Papagiannopoulou et al., 2017a). In this figure it becomes clear that climate dynamics Granger-cause monthly vegetation anomalies in most regions of the world, and the ability of the MTL model to detect deterministic relationships is evidenced. This is also confirmed by the Wilcoxon paired statistical test ($p\text{-value} < 10^{-9}$). On the other hand, the ability of the STL model to detect ~~Geanger-causal~~ Granger-causal relationships is rather limited ~~compered-compared~~ to that of the MTL model. Figure 3e depicts the result of the comparison, where in almost all regions the quantification of Granger causality of the MTL approach increases substantially compared to the one of the STL approach. Analogous to Fig. 3c, Fig. 3f compares the distributions of Granger causality (i.e., the difference in predictive performance in terms of R^2 between the full and the baseline model) between the STL and MTL approach. Once again, the blue histogram corresponds to the distribution of Granger causality retrieved using the STL approach, while the orange corresponds to the results of the MTL approach. The shift to the right of the orange histogram shows the larger ability of the MTL model to reveal Granger-causality between climate and vegetation. ~~Overall, the results presented on this section~~ Similar to the previous comparison, the Wilcoxon paired statistical test (Demšar, 2006) confirms that the results of the two approaches are overall statistically different ($p\text{-value} < 10^{-9}$). In summary, these findings highlight the potential of using the low-dimensional feature representation learned from the data to ~~fulfil~~ fulfill our final objective, which is the detection of ~~climate-vegetation-regions~~ vegetated areas holding a similar response to climate via a clustering approach.

3.2 Appropriate number of ~~the~~ hydro-climatic biomes

As described in Sect. 2.5, there are multiple approaches that can be used to define the number of classes in a clustering problem. In our framework, we define the number of clusters by using a data-driven approach. In our analysis, we choose not to use information from any pre-defined number of vegetation and/or climate classes existing in the literature, since the ultimate goal is to identify land classes fully independently, and only based on the observed relationship between vegetation and climate. To this end, we rely on the definition of the number of clusters on the predictive performance of the MTL model. In Sect. 2.3, it is stated that the ASO-MTL approach shares the objective function of the CMTL method. This only holds if the number of clusters (which is a pre-defined parameter in the CMTL method) is equal to the value of the parameter h in the ASO-MTL method, which is the dimensionality of the common feature space. In light of this equivalence relation, we experimented with a wide range of values for h in a validation set, aiming to select the value of h that maximises the model performance in terms of R^2 . As such, we conclude that the best predictive performance occurs at $h = 11$, and that the appropriate number of biomes in the clustering phase equals to 11 – see Sect. S2 of the Supplementary material for more details.

~~This analysis provides an indication about the number of clusters that emerge from the data set; the~~ The results of this hierarchical clustering (with Euclidean distance) can be visualised in a dendrogram representation, which provides an indication about the optimal number of clusters that emerge from the data set. Figure 4b depicts the dendrogram formed by our framework, with the vertical cutting line separating the data into 11 clusters. This representation allows for a visual inspection of whether the choice of ~~the number of 11~~ clusters is in line with the dissimilarities existing in the observations. As one can observe, our choice is reasonable, since the clusters at this point are quite dissimilar, based on the Euclidean distance metric, compared to

hypothesized cutting lines either before or after this point. In other words, the branches of the dendrogram are already quite
5 long at 11 clusters, indicating high dissimilarities between ~~clusters/observations~~the resulting classes.

3.3 Hydro-climatic biomes

The final objective of this study is ~~the definition of~~to uncover the regions in which vegetation responds in a analogous way to climate anomalies, here referred to as ‘hydro-climatic biomes’. In the previous section, we investigated the appropriate number of such regions based on the information contained in our database. Figure 4a illustrates the spatial distribution of the
10 emerging global hydro-climatic biomes. The colours depicted correspond to those of the clusters in the dendrogram of Fig. 4b. Further analysis of ~~the dendrogram of Fig. 4b~~this dendrogram, in combination with the spatial distribution of the clusters in Fig. 4a, shows that our framework can clearly differentiate the bio-climatic behaviour of northern latitude ecosystems from
~~the one in~~those in mid- and southern latitudes. The behaviour of tropical ecoregions is unsurprisingly closer to the behaviour of sub-tropical ones, while boreal regions sharing the exposure to low temperature anomalies have a more coherent response
15 to one another, forming the second main branch of the dendrogram. Bearing in mind the results of the Granger causality approach by Papagiannopoulou et al. (2017b), as well as the prior knowledge on climate and land use classification, we define the hydro-climatic biomes as follows: (1) Tropical, (2) Transitional water-driven, (3) Transitional energy-driven, (4) Sub-tropical energy-driven, (5) Sub-tropical water-driven, (6) Mid-latitude water-driven, (7) Mid-latitude temperature-driven, (8) Boreal temperature-driven, (9) Boreal water-driven, (10) Boreal water/temperature-driven, (11) Boreal energy-driven. This
20 nomenclature is broadly based on latitude and main climatic drivers.

Figure 4c shows the main 10 climate regions of the Köppen-Geiger climate classification, which is based on ~~climatic conditions defined by~~ precipitation and temperature, and their seasonality. On the other hand, the International Geosphere-Biosphere Program (IGBP) (Loveland and Belward, 1997) land cover classification, depicted in Fig. 4d, is mostly based on plant functional types. Without the need to prescribe any land cover or climate classification, and only relying on the spatial
25 coherence in the vegetation response to climate anomalies, our hydro-climatic biomes in Fig. 4a clearly depict some of the main characteristic patterns from these traditional classification schemes. For instance, the region of North Asia is quite coherent in terms of climate based on the 10 climate classes shown here (Fig. 4c), but quite diverse in terms of vegetation type (Fig. 4d); the hydro-climatic biomes show a clear distinction in the transition from shrublands (~~energy-driven~~energy-driven) to coniferous forests (energy- and water-driven). In North America, the more energy-limited ecosystems ~~around~~along the coasts
30 emerge from the water-driven regions inland, and a latitudinal behaviour is also depicted, partly reflecting the transition from croplands and grasslands into temperate and boreal forests. Patterns in the tropics clearly differentiate between rainforest and transitional savannahs, and in South America the different drivers of vegetation dynamics in the Arc of Deforestation lead to a class change that is not depicted by ~~either~~neither the Köppen-Geiger climate classification nor the IGBP land cover classes. Finally the patterns found for arid and warm semiarid regions (here referred to as ‘sub-tropical water-driven’), and their tran-
35 sition towards wetter and more vegetated ecosystems, agree with the expectations based on vegetation (Fig. 4d) and climate (Fig. 4c).

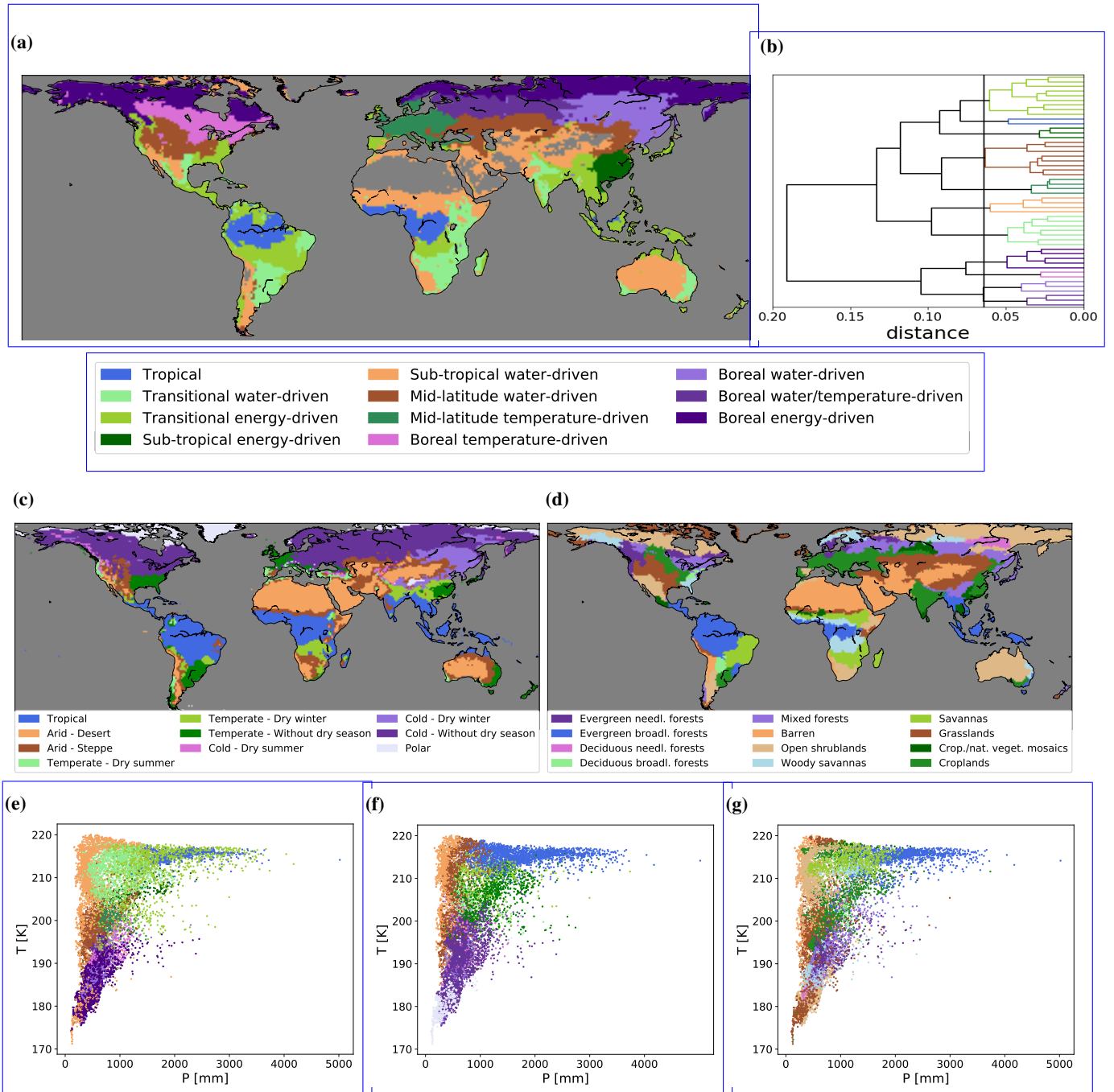


Figure 4. Comparison of the different land surface classification schemes. (a) Hydro-climatic biomes derived from the proposed framework. The region colours correspond to the colours of the clusters that are depicted in the dendrogram. (b) Dendrogram scheme of the clustering result-derived by from the hierarchical agglomerative clustering on the low-dimensional representation of our model observations. The length of the dendrogram branches is a function of the inter-cluster dissimilarities. The vertical cutting line marks the data split into 11 clusters. The denomination of the different classes is supported by the results from Papagiannopoulou et al. (2017b). (c) Simplified Köppen-Geiger climate classification scheme. (d) IGBP land use classification scheme. (e) Climate space (i.e. mean annual temperature versus precipitation) for our hydro-climatic biomes in Fig. 4a. (f) Same as (e) but for the Köppen-Geiger climate classes in Fig. 4c. (g) Same as (e) but for IGBP in Fig. 4d.

Therefore, the comparison to the Köppen-Geiger and IGBP maps serves only as a general evaluation or proof of concept for our hydro-climatic biomes map, since in the end such maps are based on a different rationale, and thus, there is no intent to 'outperform' these classification schemes. However, it can be observed in this comparison that the hydro-climatic biomes map in Fig. 4a combines information on climate and vegetation zones by illustrating regions where vegetation similarly interacts with the multi-month dynamics in climatic and environmental conditions. As such, the clustering. This conclusion is confirmed by the scatter plots in Figs. 4e-g. Figure 4e depicts our hydro-climatic biomes of Fig. 4a in climate space of mean annual temperature against precipitation, while Fig. 4f shows the same but for the Köppen-Geiger climate classes of Fig. 4c. In Fig. 4f, the five climate classes are well-separated, since their definition is based on these two climatic variables. On the other hand, Fig. 4g depicts the same information but for the IGBP map of Fig. 4d. In this figure, savannahs, tropics, and shrublands appear again well clustered. It can be observed that the scatter plot of Fig. 4e clearly lie between the two previous classifications in terms of clustering. Boreal biomes correspond to cold climate classes, the sub-tropical and mid-latitude water-driven biomes correspond to arid regions, while the transitional biomes correspond to the savannas and croplands. The clustering of biomes is also consistent with the global distribution of key climatic drivers reported by Papagiannopoulou et al. (2017b) based on random forests and a Granger-causality framework, since these biomes are ultimately defined based on the response of vegetation to climatic and environmental conditions. These common dynamics are identified by latent structures in our MTL approach. A discussion about these latent structures is included in the Supplementary material (Sect. S3). Moreover, we should note that the approach of spectral clustering applied here, allows for a robust result, as small perturbations in the data sets do not affect the overall clustering result. This conclusion is confirmed by the fact that even in the tropical region tropical regions, where the uncertainty in the observations is typically larger and the skill of the predictions is lower (see Fig. 3), the different clusters are separated in a clear manner. A discussion about the comparison of the four-three land surface classification schemes (the hydro-climatic biomes, the Köppen-Geiger climate classification, and the IGBP land use classification and global distribution of key climatic drivers derived by the non-linear Granger-causality framework) based on the predictive structures is presented in Sect. S4 of the Supplementary material. Results for microwave vegetation optical depth (VOD) (Liu et al., 2011) anomalies as alternative to NDVI anomalies are consistent as shown in Supplementary material Fig. S7.

4 Conclusion

In this paper we introduced a novel framework for identifying regions with similar biosphere-climate dynamics interplay. Our framework combines a multi-task learning (MTL) modelling approach and a spectral clustering technique, and it is applied to the a global database of global observational climate records compiled by Papagiannopoulou et al. (2017a). Comparisons to a typical single-task learning approach, in which each task (in each location) is analysed separately, indicate that learning about climate-vegetation-climate-vegetation relationships in neighbouring, or even remote, locations can help predict local vegetation dynamics based on climate variability. Moreover, our approach is able to detect shared hidden predictive structures among the tasks that enhance the predictive performance of the models. These predictive structures form the basis to which the clustering

algorithm is applied to detect regions where vegetation responds to climate in a similar way. We demonstrate that, without the need to prescribe any land cover information, our method is able to identify coherent ~~climate-vegetation~~ climate-vegetation interaction zones that emerge directly from the spatio-temporal variability in the data. These zones agree with traditional global classification maps, such as the Köppen-Geiger climate classification or the IGBP land cover classification. We refer to these regions as ‘hydro-climatic biomes’. These ~~wider-wide~~ regions can be used in various applications in geosciences, such as unravelling anomalous relationships between climate and vegetation dynamics at local scales, defining extreme values of
5 vegetation response to climate, exploring tipping points and turning points (Horion et al., 2016) of ecosystem resilience, and benchmarking the dynamic response of vegetation in Earth system models.

Code and data availability. We use the implementation of Python for the L-BFGS optimizer, the singular value decomposition method and the hierarchical clustering (scikit-learn python library (Pedregosa et al., 2011)). The code for the ASO-MTL method has been uploaded to our github repository (<https://github.com/lhwm/hydro-climatic-biomes>). Data used in this manuscript can be accessed using <http://www.SAT-EX.ugent.be> as gateway.
10

Author contributions. Christina Papagiannopoulou, Willem Waegeman and Diego G. Miralles conceived the study. Christina Papagiannopoulou conducted the analysis. Christina Papagiannopoulou, Diego G. Miralles and Matthias Demuzere led the writing. All co-authors contributed to the design of the experiments, discussion and interpretation of results, and editing of the manuscript.

Acknowledgements. This work is funded by the Belgian Science Policy Office (BELSPO) in the framework of the STEREO III programme,
15 project SAT-EX (SR/00/306). D. G. Miralles acknowledges support from the European Research Council (ERC) under grant agreement no. 715254 (DRY-2-DRY). The authors thank Stijn Decubber for fruitful discussions. ~~Finally, the authors~~ The authors also sincerely thank the individual developers of the wide range of global data sets used in this study. Finally, the authors thank the reviewers for their constructive feedback.

References

- 20 Ando, R. K. and Zhang, T.: A framework for learning predictive structures from multiple tasks and unlabeled data, *Journal of Machine Learning Research*, 6, 1817–1853, 2005.
- Baker, B., Diaz, H., Hargrove, W., and Hoffman, F.: Use of the Köppen–Trewartha climate classification to evaluate climatic refugia in statistically derived ecoregions for the People’s Republic of China, *Climatic Change*, 98, 113, <https://doi.org/10.1007/s10584-009-9622-2>, 2009.
- 25 Bartholomé, E. and Belward, A. S.: GLC2000: a new approach to global land cover mapping from Earth observation data, *Int. J. Remote Sens.*, 26, 1959–1977, 2005.
- Barzilai, A. and Crammer, K.: Convex multi-task learning by clustering, in: *Artificial Intelligence and Statistics*, pp. 65–73, 2015.
- Baxter, J.: A Bayesian/information theoretic model of learning to learn via multiple task sampling, *Machine learning*, 28, 7–39, 1997.
- Baxter, J. et al.: A model of inductive bias learning, *J. Artif. Intell. Res. (JAIR)*, 12, 3, 2000.
- 30 Benjamini, Y. and Hochberg, Y.: Controlling the False Discovery Rate: A Practical and Powerful Approach to Multiple Testing, *Journal of the Royal Statistical Society. Series B (Methodological)*, 57, 289–300, 1995.
- Bi, J., Xiong, T., Yu, S., Dundar, M., and Rao, R. B.: An improved multi-task learning approach with applications in medical diagnosis, in: *Joint European Conference on Machine Learning and Knowledge Discovery in Databases*, pp. 117–132, Springer, 2008.
- Brugger, K. and Rubel, F.: Characterizing the species composition of European Culicoides vectors by means of the Köppen–Geiger climate classification, *Parasites & vectors*, 6, 333, 2013.
- 35 Brunsdon, C., Fotheringham, A. S., and Charlton, M. E.: Geographically Weighted Regression: A Method for Exploring Spatial Nonstationarity, *Geographical Analysis*, 28, 281–298, <https://doi.org/10.1111/j.1538-4632.1996.tb00936.x>, 1996.
- Caruana, R.: Multitask Learning, *Machine Learning*, 28, 41–75, <https://doi.org/10.1023/A:1007379606734>, 1997.
- Chan, D. and Wu, Q.: Significant anthropogenic-induced changes of climate classes since 1950, *Sci. Rep.*, 5, 13 487, <https://doi.org/10.1038/srep13487>, 2015.
- 5 Chen, D. and Chen, H. W.: Using the Köppen classification to quantify climate variation and change: an example for 1901–2010, *Environmental Development*, 6, 69–79, 2013.
- Chen, J., Tang, L., Liu, J., and Ye, J.: A convex formulation for learning shared structures from multiple tasks, in: *26th Annual International Conference on Machine Learning*, pp. 137–144, ACM, 2009.
- Chen, S. and Tian, Y.: Pyramid of spatial relations for scene-level land use classification, *IEEE Trans. Geosci. Remote Sens.*, 53, 1947–1957, 10 2015.
- Congalton, R. G., Gu, J., Yadav, K., Thenkabail, P., and Ozdogan, M.: Global land cover mapping: A review and uncertainty analysis, *Remote Sens.*, 6, 12 070–12 093, 2014.
- De Keersmaecker, W., Lhermitte, S., Tits, L., Honnay, O., Somers, B., and Coppin, P.: A model quantifying global vegetation resistance and resilience to short-term climate anomalies and their relationship with vegetation cover, *Global Ecology and Biogeography*, 24, 539–548, 15 <https://doi.org/10.1111/geb.12279>, 2015.
- Demšar, J.: Statistical comparisons of classifiers over multiple data sets, *Journal of Machine Learning Research*, 7, 1–30, 2006.
- Diaz, H. F. and Eischeid, J. K.: Disappearing “alpine tundra” Köppen climatic type in the western United States, *Geophys. Res. Lett.*, 34, 2007.

- Diebold, F. X.: Comparing Predictive Accuracy, Twenty Years Later: A Personal Perspective on the Use and Abuse of Diebold–Mariano Tests, *Journal of Business & Economic Statistics*, 33, 1–1, <https://doi.org/10.1080/07350015.2014.983236>, 2015.
- Faghmous, J. H. and Kumar, V.: A Big Data Guide to Understanding Climate Change: The Case for Theory-Guided Data Science., *Big Data*, 2, 155–163, <https://doi.org/10.1089/big.2014.0026>, 2014.
- Feddema, J. J.: A Revised Thornthwaite-Type Global Climate Classification, *Physical Geography*, 26, 442–466, <https://doi.org/10.2747/0272-3646.26.6.442>, 2005.
- 25 Feddema, J. J., Oleson, K. W., Bonan, G. B., Mearns, L. O., Buja, L. E., Meehl, G. A., and Washington, W. M.: Atmospheric science: The importance of land-cover change in simulating future climates, *Science*, 310, 1674–1678, <https://doi.org/10.1126/science.1118160>, 2005.
- Gallardo, C., Gil, V., Hagel, E., Tejeda, C., and de Castro, M.: Assessment of climate change in Europe from an ensemble of regional climate models by the use of Köppen–Trewartha classification, *Int. J. Climatol.*, 33, 2157–2166, 2013.
- Garcia, R. A., Cabeza, M., Rahbek, C., and Araújo, M. B.: Multiple dimensions of climate change and their implications for biodiversity, *Science*, 344, 1247–1252, 2014.
- 30 Georganos, S., Abdi, A. M., Tenenbaum, D. E., and Kalogirou, S.: Examining the NDVI-rainfall relationship in the semi-arid Sahel using geographically weighted regression, *Journal of Arid Environments*, 146, 64 – 74, <https://doi.org/https://doi.org/10.1016/j.jaridenv.2017.06.004>, 2017.
- Gonçalves, A. R., Banerjee, A., and Von Zuben, F. J.: Spatial Projection of Multiple Climate Variables Using Hierarchical Multitask Learning., in: *AAAI Conference on Artificial Intelligence*, pp. 4509–4515, 2017.
- 35 Hanf, F., Körper, J., Spangehl, T., and Cubasch, U.: Shifts of climate zones in multi-model climate change experiments using the Köppen climate classification, *Meteorol. Z.*, 21, 111–123, 2012.
- Herrando-Pérez, S., Delean, S., Brook, B. W., Cassey, P., and Bradshaw, C. J.: Spatial climate patterns explain negligible variation in strength of compensatory density feedbacks in birds and mammals, *PLoS One*, 9, e91536, 2014.
- Horion, S., Prishchepov, A. V., Verbesselt, J., Beurs, K., Tagesson, T., and Fensholt, R.: Revealing turning points in ecosystem functioning over the Northern Eurasian agricultural frontier, *Global Change Biology*, 22, 2801–2817, <https://doi.org/10.1111/gcb.13267>, 2016.
- 5 Ivits, E., Horion, S., Fensholt, R., and Cherlet, M.: Global Ecosystem Response Types Derived from the Standardized Precipitation Evapotranspiration Index and FPAR3g Series, *Remote Sensing*, 6, 4266–4288, <https://doi.org/10.3390/rs6054266>, 2014.
- Jacob, L., Vert, J.-p., and Bach, F. R.: Clustered multi-task learning: A convex formulation, in: *Advances in Neural Information Processing systems*, pp. 745–752, 2009.
- Köppen, W.: *Das Geographische System der Klimate*, *Handbuch der klimatologie*, 1, 1936.
- 10 Kottek, M., Grieser, J., Beck, C., Rudolf, B., and Rubel, F.: World map of the Köppen-Geiger climate classification updated, *Meteorol. Z.*, 15, 259–263, 2006.
- Li, W., MacBean, N., Ciais, P., Defourny, P., Lamarche, C., Bontemps, S., Houghton, R. A., and Peng, S.: Gross and net land cover changes in the main plant functional types derived from the annual ESA CCI land cover maps (1992–2015), *Earth Syst. Sci. Data*, 10, 219–234, <https://doi.org/10.5194/essd-10-219-2018>, 2018.
- 15 Liu, L., Zhang, Y., Wu, S., Li, S., and Qin, D.: Water memory effects and their impacts on global vegetation productivity and resilience, *Scientific reports*, 8, 2962, 2018.
- Liu, Y. Y., de Jeu, R. A. M., McCabe, M. F., Evans, J. P., and van Dijk, A. I. J. M.: Global long-term passive microwave satellite-based retrievals of vegetation optical depth, *Geophysical Research Letters*, 38, <https://doi.org/10.1029/2011GL048684>, 2011.

- Loveland, T. and Belward, A.: The IGBP-DIS global 1km land cover data set, DISCover: first results, *Int. J. Remote Sens.*, 18, 3289–3295, 1997.
- Loveland, T. R., Reed, B. C., Brown, J. F., Ohlen, D. O., Zhu, Z., Yang, L., and Merchant, J. W.: Development of a global land cover characteristics database and IGBP DISCover from 1 km AVHRR data, *Int. J. Remote Sens.*, 21, 1303–1330, 2000.
- Lund, R. and Li, B.: Revisiting climate region definitions via clustering, *J. Climate*, 22, 1787–1800, 2009.
- Mahlstein, I., Daniel, J. S., and Solomon, S.: Pace of shifts in climate regions increases with global temperature, *Nature Climate Change*, 3, 739, 2013.
- McQuade, S. and Monteleoni, C.: MRF-Based Spatial Expert Tracking of the Multi-Model Ensemble, in: *International Workshop on Climate Informatics*, 2013.
- Mekhalfi, M. L., Melgani, F., Bazi, Y., and Alajlan, N.: Land-use classification with compressive sensing multifeature fusion, *IEEE Geosci. Remote Sens. Lett.*, 12, 2155–2159, 2015.
- Metzger, M. J., Bunce, R. G. H., Jongman, R. H. G., Sayre, R., Trabucco, A., and Zomer, R.: A high-resolution bioclimate map of the world: a unifying framework for global biodiversity research and monitoring, *Global Ecology and Biogeography*, 22, 630–638, <https://doi.org/10.1111/geb.12022>, 2012.
- Nemani, R. R., Keeling, C. D., Hashimoto, H., Jolly, W. M., Piper, S. C., Tucker, C. J., Myneni, R. B., and Running, S. W.: Climate-driven increases in global terrestrial net primary production from 1982 to 1999, *Science*, 300, 1560–1563, 2003.
- Netzel, P. and Stepinski, T.: On using a clustering approach for global climate classification, *J. Climate*, 29, 3387–3401, 2016.
- Netzel, P. and Stepinski, T. F.: World Climate Search and Classification Using a Dynamic Time Warping Similarity Function, in: *Advances in Geocomputation*, pp. 181–195, Springer, 2017.
- Ng, A. Y., Jordan, M. I., and Weiss, Y.: On spectral clustering: Analysis and an algorithm, in: *Advances in Neural Information Processing systems*, pp. 849–856, 2002.
- Papagiannopoulou, C., Miralles, D. G., Decubber, S., Demuzere, M., Verhoest, N. E. C., Dorigo, W. A., and Waegeman, W.: A non-linear Granger-causality framework to investigate climate–vegetation dynamics, *Geosci. Model Dev.*, 10, 1945–1960, <https://doi.org/10.5194/gmd-10-1945-2017>, 2017a.
- Papagiannopoulou, C., Miralles, D. G., Dorigo, W. A., Verhoest, N. E. C., Depoorter, M., and Waegeman, W.: Vegetation anomalies caused by antecedent precipitation in most of the world, *Environ. Res. Lett.*, 12, 074 016, <https://doi.org/10.1088/1748-9326/aa7145>, 2017b.
- Pedregosa, F., Varoquaux, G., Gramfort, A., Michel, V., Thirion, B., Grisel, O., Blondel, M., Prettenhofer, P., Weiss, R., Dubourg, V., Vanderplas, J., Passos, A., Cournapeau, D., Brucher, M., Perrot, M., and Duchesnay, E.: Scikit-learn: Machine Learning in Python, *Journal of Machine Learning Research*, 12, 2825–2830, 2011.
- Peel, M. C., Finlayson, B. L., and McMahon, T. A.: Updated world map of the Köppen-Geiger climate classification, *Hydrol. Earth Syst. Sci. Discuss.*, 4, 439–473, 2007.
- Poulter, B., MacBean, N., Hartley, A., Khlystova, I., Arino, O., Betts, R., Bontemps, S., Boettcher, M., Brockmann, C., Defourny, P., Hagemann, S., Herold, M., Kirches, G., Lamarche, C., Lederer, D., Ottlé, C., Peters, M., and Peylin, P.: Plant functional type classification for earth system models: Results from the European Space Agency’s Land Cover Climate Change Initiative, *Geosci. Model Dev.*, 8, 2315–2328, <https://doi.org/10.5194/gmd-8-2315-2015>, 2015.
- Propastin, P., Kappas, M., and Erasmi, S.: Application of Geographically Weighted Regression to Investigate the Impact of Scale on Prediction Uncertainty by Modelling Relationship between Vegetation and Climate., *International Journal of Spatial Data Infrastructures Research*, 3, 73–94, 2008.

- Scott, G. J., England, M. R., Starms, W. A., Marcum, R. A., and Davis, C. H.: Training deep convolutional neural networks for land–cover classification of high-resolution imagery, *IEEE Geosci. Remote Sens. Lett.*, 14, 549–553, 2017.
- Seddon, A. W., Macias-Fauria, M., Long, P. R., Benz, D., and Willis, K. J.: Sensitivity of global terrestrial ecosystems to climate variability, *Nature*, 531, 229, 2016.
- Spinoni, J., Vogt, J., Naumann, G., Carrao, H., and Barbosa, P.: Towards identifying areas at climatological risk of desertification using the Köppen–Geiger classification and FAO aridity index, *Int. J. Climatol.*, 35, 2210–2222, 2015.
- 25 Subbian, K. and Banerjee, A.: Climate multi-model regression using spatial smoothing, in: *SIAM International Conference on Data Mining*, pp. 324–332, SIAM, 2013.
- Thornthwaite, C. W.: Problems in the classification of climates, *Geographical Review*, 33, 233–255, 1943.
- Trewartha, G. and Horn, L.: *An Introduction to Climate* –McGraw-Hill, New York, 416pp, 1980.
- Tucker, C. J., Pinzon, J. E., Brown, M. E., Slayback, D. A., Pak, E. W., Mahoney, R., Vermote, E. F., and El Saleous, N.: An extended AVHRR 8-km NDVI dataset compatible with MODIS and SPOT vegetation NDVI data, *Int. J. Remote Sens.*, 26, 4485–4498, 2005.
- 30 Wang, F., Wang, X., and Li, T.: Semi-supervised multi-task learning with task regularizations, in: *9th IEEE International Conference on Data Mining (ICDM'09)*, pp. 562–568, IEEE, 2009.
- Ward, J. H.: Hierarchical Grouping to Optimize an Objective Function, *Journal of the American Statistical Association*, 58, 236–244, <https://doi.org/10.1080/01621459.1963.10500845>, 1963.
- 35 Xu, D. and Tian, Y.: A Comprehensive Survey of Clustering Algorithms, *Annals of Data Science*, 2, 165–193, <https://doi.org/10.1007/s40745-015-0040-1>, 2015.
- Xu, J., Tan, P.-N., Luo, L., and Zhou, J.: Gspartan: a geospatio-temporal multi-task learning framework for multi-location prediction, in: *SIAM International Conference on Data Mining*, pp. 657–665, SIAM, 2016.
- Xu, X., Li, W., Ran, Q., Du, Q., Gao, L., and Zhang, B.: Multisource Remote Sensing Data Classification Based on Convolutional Neural Network, *IEEE Trans. Geosci. Remote Sens.*, 56, 937–949, <https://doi.org/10.1109/TGRS.2017.2756851>, 2018.
- Xue, Y., Liao, X., Carin, L., and Krishnapuram, B.: Multi-task learning for classification with dirichlet process priors, *Journal of Machine Learning Research*, 8, 35–63, 2007.
- 590 Zhang, D., Shen, D., Initiative, A. D. N., et al.: Multi-modal multi-task learning for joint prediction of multiple regression and classification variables in Alzheimer’s disease, *Neuroimage*, 59, 895–907, 2012.
- Zhang, X. and Yan, X.: Spatiotemporal change in geographical distribution of global climate types in the context of climate warming, *Climate Dyn.*, 43, 595–605, 2014a.
- 595 Zhang, X. and Yan, X.: Temporal change of climate zones in China in the context of climate warming, *Theor. Appl. Climatol.*, 115, 167–175, 2014b.
- Zhang, Z., Luo, P., Loy, C. C., and Tang, X.: Facial landmark detection by deep multi-task learning, in: *European Conference on Computer Vision*, pp. 94–108, Springer, 2014.
- Zhao, Z., Gao, J., Wang, Y., Liu, J., and Li, S.: Exploring spatially variable relationships between NDVI and climatic factors in a transition zone using geographically weighted regression, *Theoretical and Applied Climatology*, 120, 507–519, 2015.
- 600 Zhou, J., Chen, J., and Ye, J.: Clustered multi-task learning via alternating structure optimization, in: *Advances in Neural Information Processing systems*, pp. 702–710, 2011.
- Zscheischler, J., Mahecha, M. D., and Harmeling, S.: Climate classifications: the value of unsupervised clustering, *Procedia Comput. Sci.*, 9, 897–906, 2012.

Supplement of “Global hydro-climatic biomes identified via multi-task learning”

Christina Papagiannopoulou¹, Diego G. Miralles², Matthias Demuzere², Niko E. C. Verhoest², and Willem Waegeman¹

¹Depart. of Data Analysis and Mathematical Modelling, Ghent University, Belgium,

²Laboratory of Hydrology and Water Management, Ghent University, Belgium

Correspondence: Christina Papagiannopoulou (christina.papagiannopoulou@ugent.be)

S1 Importance of a higher-level representation of features

To illustrate the non-linear response of vegetation and explain our choice to use high-level feature representation in our framework, we compare the model performance with and without the use of this high-level representation. Figure S1a shows the predictive performance of the Alternative Structure Optimization multi-task [learning](#) (ASO-MTL) method when the raw variables as well as the corresponding 6-lagged values are included in the model, i.e., the cumulative variables and the extreme indices are not included as predictors. Figure S1b visualizes the difference in predictive performance of the ASO-MTL model with and without the cumulative variables and the extreme indices as predictors. As one can observe, in regions such as Europe, North America, southern and northern parts of Asia and parts of South America, the model performance substantially decreases if these higher-level features are not used in the data representation. In these regions, more than 10% of the variability in NDVI anomalies is explained by this more complex (non-linear) representation, illustrating the non-linear nature of the relationship between climate and vegetation dynamics.

S2 Number of hydro-climatic biomes

Figure S2 shows the median of the predictive performance (R^2) for all tasks when the value of the parameter h varies. Note that for these experiments, the λ parameters remain constant in order to assess only the effect of parameter h on the model performance. As one can observe in Fig. S2, the maximum median value R^2 is achieved when $h = 11$. However, the differences in the predictive performance for $h = 6, \dots, 15$ are marginal. Therefore, we can conclude that the method gives robust results as the strongest predictive structures are captured for the first most important components given by the singular value decomposition. [This conclusion is also confirmed by Fig. S3, where the maps with 9 \(Fig. S3a\), 10 \(Fig. S3b\), 11 \(Fig. S3c\) and 12 \(Fig. S3d\) hydro-climatic biomes are depicted. In all figures, the tropics, the boreal and the arid regions are well-detected. In addition, sub-tropical regions and transitional ones are also commonly defined in all of the aforementioned figures. Differences in the borders of the identified regions are noticed between temperature-driven areas \(e.g., Europe and North America\). In transitional](#)

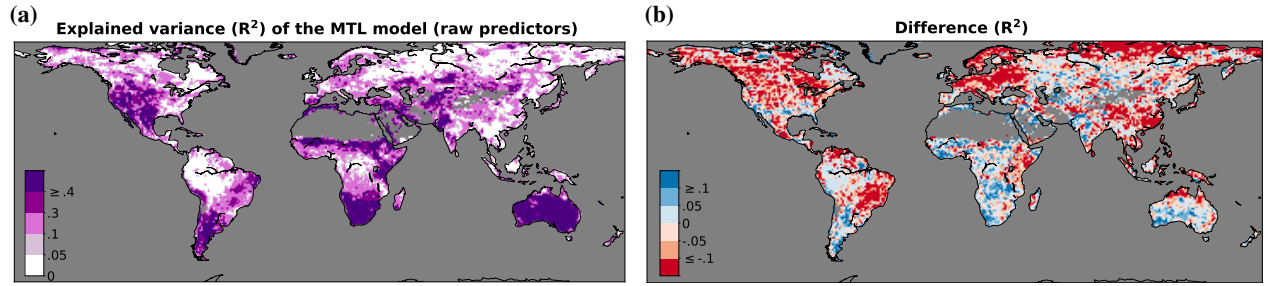


Figure S1. Comparison of the predictive performance in terms of R^2 of the model which does not include the cumulative variables and the extreme indices with the model which is trained with the full collection of higher-level features (Papagiannopoulou et al., 2017a). (a) Explained variance (R^2) of NDVI anomalies based on the raw data of the climatic variables as well as their 6-lagged values (cumulative variables and the extreme indices are not included as predictors to the model). (b) Difference in terms of R^2 between the model without cumulative and extreme predictors and the model which includes all the higher-level feature representation in Fig. 3a of the manuscript.

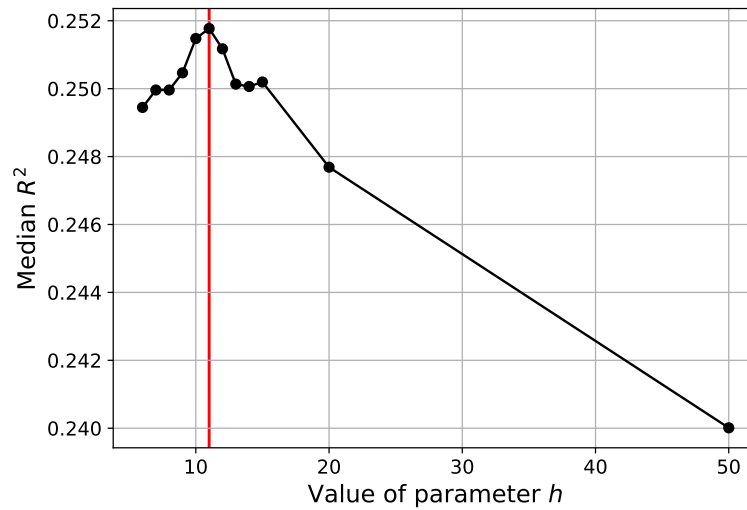


Figure S2. Assessing the number of biomes: Median of the predictive performance of the ASO-MTL model in terms of R^2 when the value of the h parameter varies. For $h = 11$ the model scores the maximum value of R^2 . However, the differences in the predictive performance for $h = 6, \dots, 15$ are marginal.

water- and energy-driven regions also there are some differences in the clusters' borders. However, these inconsistencies can be explained by the smoother differences between the climatic and environmental conditions in these areas.

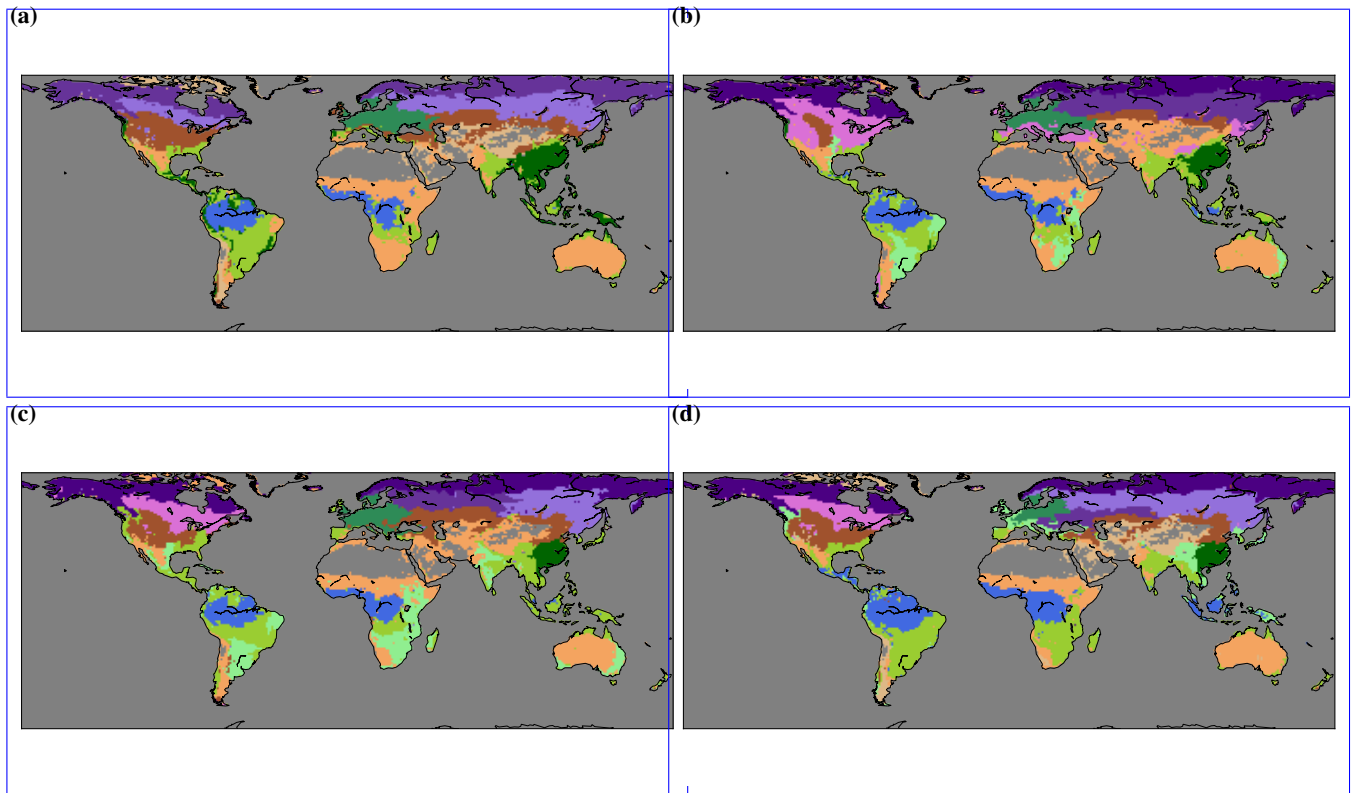


Figure S3. Maps with different number of hydro-climatic biomes. (a) $h = 9$ (i.e., 9 hydro-climatic biomes), (b) $h = 10$, (c) $h = 11$ (Fig. 4a of the manuscript), and (d) $h = 12$.

S3 Visualization of the most important predictive structures

In Sect. 2.5 of the manuscript, we describe the steps of the SVD-based ASO algorithm, which learns a low-dimensional feature representation for our tasks based on the relationships between them. The learned matrix Θ maps the high-dimensional space to a (lower) h -dimensional space, storing the loads of the original weights to the “highly predictive structures”. Thus, the task models are also projected to this shared lower-dimensional space. This information is stored in the matrix \mathbf{V} on which the clustering approach is performed. Figure S4 presents the values of the tasks in the first 6 components of the matrix \mathbf{V} . Similar pixel values to the same components mean similar ~~climate-vegetation~~climate-vegetation dynamics. There are several remarks considering Fig. S4: (1) all the 6 components are able to distinguish specific regions according to different criteria such as regions with temperate and dry climate, regions with cold and dry climate, tropical and dry climate, etc.; (2) pixels which are grouped into the same region in the final clustering result (Fig. 4a of the manuscript) tend to have similar values in a particular

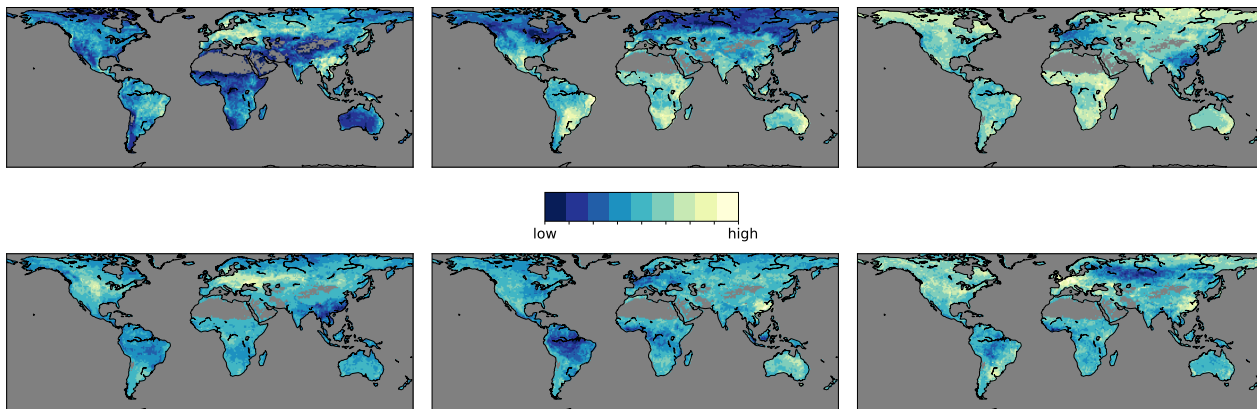


Figure S4. Visualization of the first 6 “principal components” of the predictive structures. The classification of the land surface into the hydro-climatic biomes is based on the importance of these structures for each location. The color intensity in the map indicates the value magnitude of each pixel in a particular predictive structure.

predictive structure, and (3) the differences in the values across regions are intense, and in some cases one can recognize the boundaries of the regions depicted in Fig. 4a of the manuscript.

S4 Visualization of the predictive structures with the different land surface classifications

As in Zscheischler et al. (2012), we conduct a dimensionality reduction to the matrix V which contains the clustering data. We separately present the results for the Northern and the Southern Hemisphere (ibid.) – see Figs. S5 and S6, respectively. The data is projected onto the first 2 ~~principal components~~ components of the t-SNE method (Maaten and Hinton, 2008) and visualized based on the ~~Köppen-Geiger clustering (Köppen, 1936)~~ hydro-climatic biomes (Fig.S5e and S6e a and S6a), the ~~IGBP clustering (Loveland and Belward, 1997)~~ Köppen-Geiger clustering (Köppen, 1936) (Fig.S5d and S6d), ~~the Granger-causality result which illustrates the main climatic drivers of each region presented in Papagiannopoulou et al. (2017b)~~ (Fig.S5b and S6b) and the ~~hydro-climatic biomes~~ IGBP clustering (Loveland and Belward, 1997) (Fig.S5a and S6a c and S6c). We use the same color representation as in Fig. 4a of the manuscript. That way we can assess if the learned predictive structures match well the classes of the different classification schemes.

Considering Fig. S5, one can see that the best-formed clusters are depicted in Fig. S5a, as the clustering has been performed on this dataset (as expected). Figure S5a ~~is mostly similar to Fig. S5d which~~ c represents the IGBP land use classification; the tropical regions are well-detected as well as the forest- and the cropland-covered regions. This means that the learned predictive

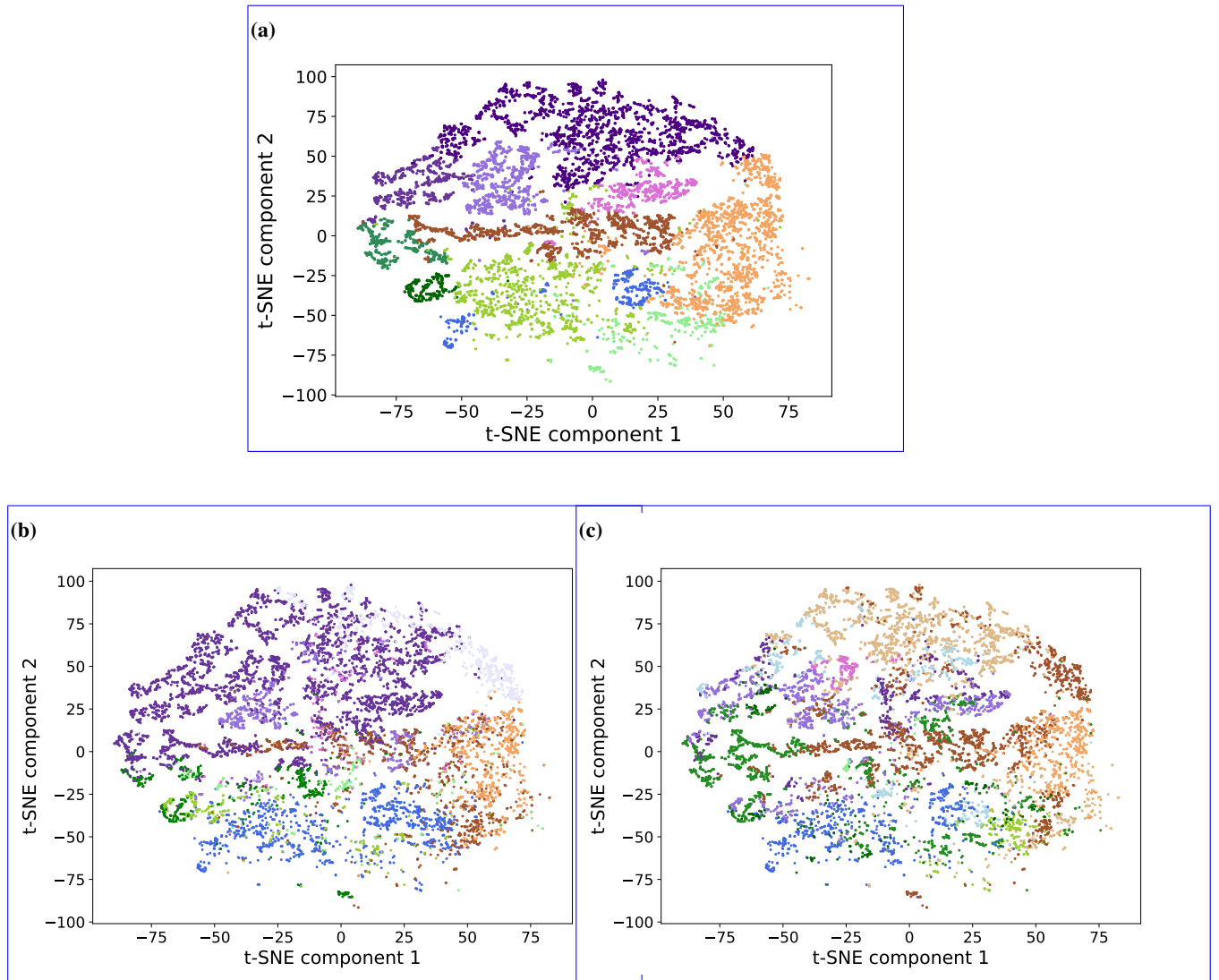


Figure S5. Data projection to the first 2 principal two t-SNE components for the Northern Hemisphere. Each point represents one pixel of the global grid and it is colored based on (a) the hydro-climatic biomes, (b) the Granger-causality classification, (c) the Köppen-Geiger climate classification, and (d) the IGBP land use classification. For the color-class mapping see Fig. 4 of the manuscript.

structures are highly relevant to the vegetation type of each region. ~~On the other hand~~In addition, Fig. S5e-b indicates that the cold, the arid and the tropical regions can be well distinguished by the learned structures whereas the temperate climate is scattered among the others and is thus harder to identify. ~~Finally, the clustering based on the main drivers, in Fig. S5b, is more scattered than the others. However, one can clearly distinguish the water-driven regions from the radiation/temperature-driven ones. This result comes from the fact that the two latter drivers (radiation and temperature) are highly correlated.~~be identified.

Figure S6 depicts the same plots for the Southern Hemisphere. As in Zscheischler et al. (2012), overall, the classes identified by the various classification schemes show a worse match than for the Northern Hemisphere. However, Fig. S6a shows that the predictive structures can clearly distinguish the sub-tropical water-driven region and the transitional energy/water-driven regions as well. In addition, the Köppen-Geiger climate classes (Fig. S6e**b**) of the tropic and the arid regions are also identified in a certain degree. The IGBP classes, in Fig S6**d**c, do not form clear clustersin the plot. Finally, one can notice that the water-driven class based on Granger causality is well separated since water is the most dominant factor in the Southern Hemisphere while energy/temperature-driven regions are rather limited.

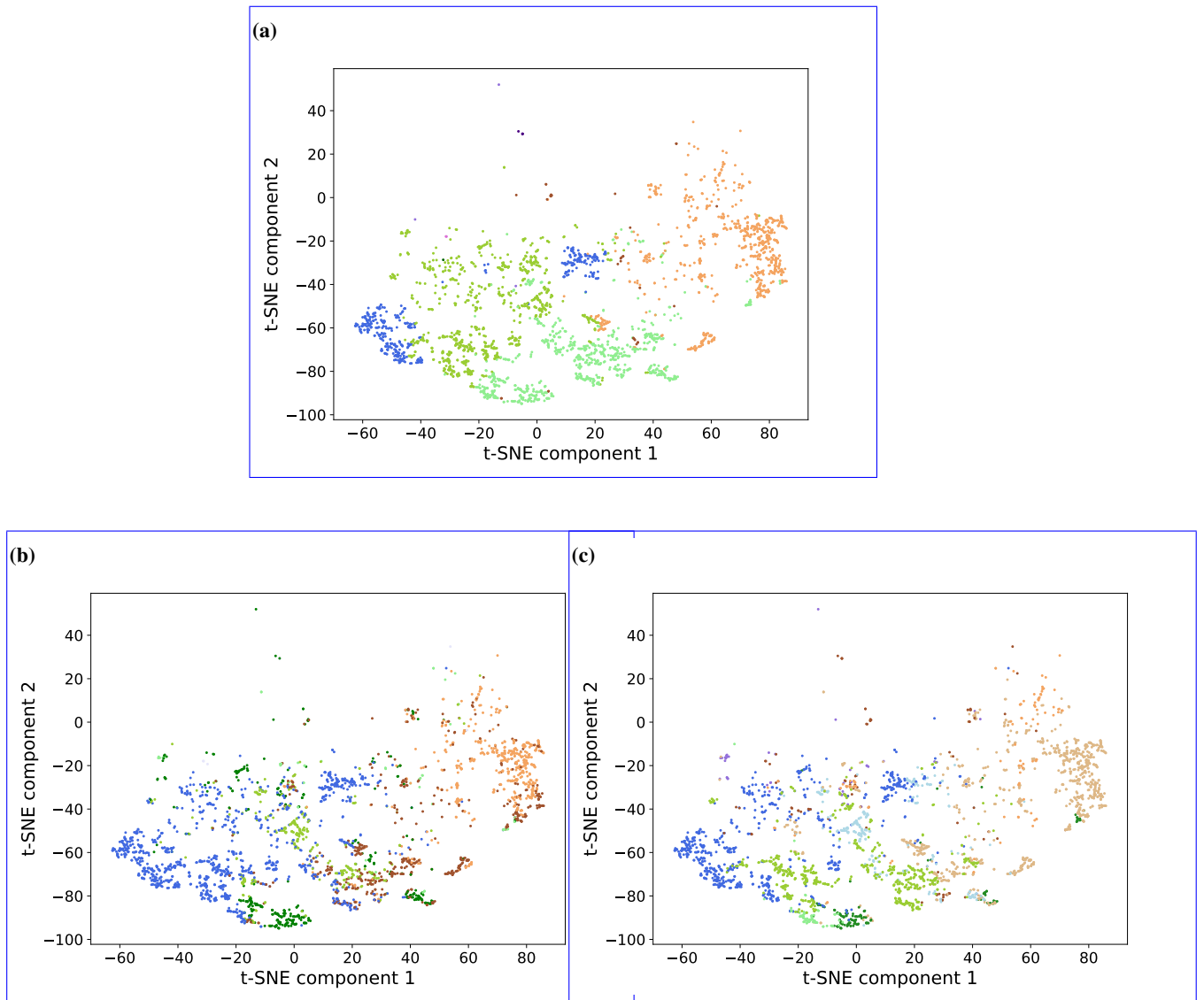


Figure S6. As Fig. S5 but for the Southern Hemisphere.

References

Köppen, W.: Das Geographische System der Klimate, Handbuch der klimatologie, 1, 1936.

Loveland, T. and Belward, A.: The IGBP-DIS global 1km land cover data set, DISCover: first results, Int. J. Remote Sens., 18, 3289–3295, 1997.

Maaten, L. v. d. and Hinton, G.: Visualizing data using t-SNE, Journal of Machine Learning Research, 9, 2579–2605, 2008.

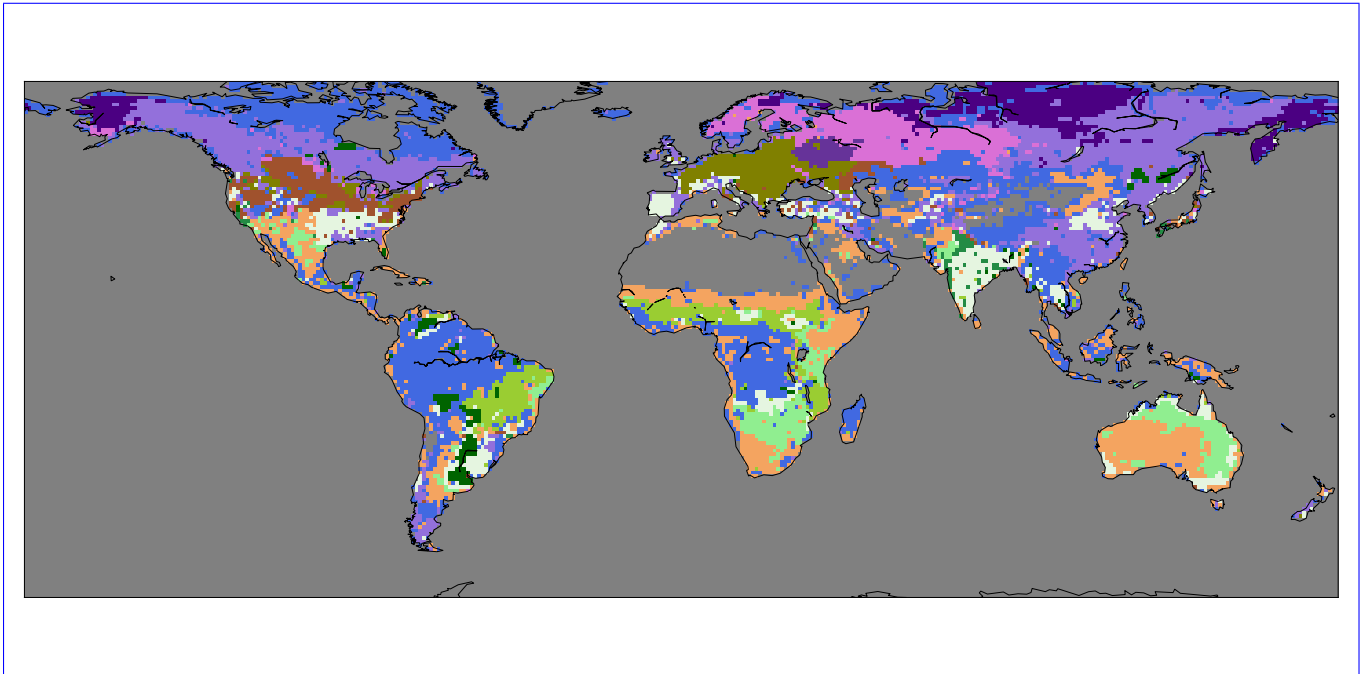


Figure S7. Hydro-climatic biomes based on vegetation optical depth (VOD) data. The VOD anomalies used as target variable in the proposed approach.

Papagiannopoulou, C., Miralles, D. G., Decubber, S., Demuzere, M., Verhoest, N. E. C., Dorigo, W. A., and Waegeman, W.: A non-linear Granger-causality framework to investigate climate–vegetation dynamics, *Geosci. Model Dev.*, 10, 1945–1960, <https://doi.org/10.5194/gmd-10-1945-2017>, 2017a.

- 5 Papagiannopoulou, C., Miralles, D. G., Dorigo, W. A., Verhoest, N. E. C., Depoorter, M., and Waegeman, W.: Vegetation anomalies caused by antecedent precipitation in most of the world, *Environ. Res. Lett.*, 12, 074 016, <https://doi.org/10.1088/1748-9326/aa7145>, 2017b.

Zscheischler, J., Mahecha, M. D., and Harmeling, S.: Climate classifications: the value of unsupervised clustering, *Procedia Comput. Sci.*, 9, 897–906, 2012.